# Multivariate Functional Brain Imaging Signatures of Cardiovascular Reactivity During Psychological Stress

by

**Thomas Edward Kraynak**

BA in Psychology, Case Western Reserve University, 2011

BM in Piano Performance, Cleveland Institute of Music, 2011

MS in Biological and Health Psychology, University of Pittsburgh, 2018

Submitted to the Graduate Faculty of the

Dietrich School of Arts and Sciences in partial fulfillment

of the requirements for the degree of

Doctor of Philosophy

University of Pittsburgh

2021

UNIVERSITY OF PITTSBURGH

DIETRICH SCHOOL OF ARTS AND SCIENCES

This dissertation was presented

by

**Thomas Edward Kraynak**

It was defended on

November 30, 2021

and approved by

Marc Coutanche, Associate Professor, Department of Psychology, University of Pittsburgh

Anna Marsland, Professor, Department of Psychology, University of Pittsburgh

Timothy Verstynen, Associate Professor, Department of Psychology, Carnegie Mellon University

Tor Wager, Distinguished Professor, Department of Psychological and Brain Sciences, Dartmouth College

Dissertation Chair: Peter Gianaros, Professor, Department of Psychology, University of Pittsburgh

**Multivariate Functional Brain Imaging Signatures of**

**Cardiovascular Reactivity During Psychological Stress**

Thomas Edward Kraynak, PhD

University of Pittsburgh, 2021

Cardiovascular reactions to psychological stressors are associated with cardiovascular disease (CVD) risk. Human brain imaging studies have identified brain regions and systems implicated in generating and regulating stressor-evoked cardiovascular reactivity, yet the reliability and generalizability of these findings remain unclear. Predictive modeling using multivariate and machine learning approaches has the promise of developing signatures of brain activity that can reliably predict outcomes, yet few studies have applied these approaches toward identifying signatures of stressor-evoked cardiovascular reactivity. Thus, the aims of the present study were (1) to develop novel multivariate signatures of stressor-evoked brain activity that could reliably predict concurrent cardiovascular physiology during stress within individuals, and (2) to evaluate whether previously reported brain signatures of cardiovascular reactivity generalize to new individuals, stressor contexts, and measures of cardiovascular physiology. Participants were 242 midlife adults (118 men and 124 women; age 30 to 51 years; 71% white) without psychiatric, immune, or cardiovascular diagnoses. Participants completed two validated cognitive stressor tasks during functional magnetic resonance imaging (fMRI) and concurrent monitoring of systolic blood pressure (SBP) and heart rate (HR). Multivariate machine learning models combining dimensionality reduction, regularized regression, and cross-validation were used to predict within-participant changes in SBP and HR during stress. Separately, two previously published multivariate signatures were applied to maps of stressor-evoked brain activity to predict SBP and

HR. Contrary to hypotheses and prior reports, multivariate patterns of stressor-evoked brain activity did not reliably predict changes in SBP and HR during stress. Notwithstanding their unreliable prediction of SBP and HR, brain activity patterns relating to SBP and HR were comprised of brain regions implicated in psychological stress and physiological control processes. In addition, two previously published multivariate brain signatures of stressor-evoked cardiovascular reactivity were found to modestly predict changes in SBP and HR during stress. These findings extend our understanding of the reliability and stability of fMRI-based signatures reflecting brain processes that may link stressful experiences to CVD risk.

## Table of Contents

## List of Tables

## List of Figures

## Acknowledgements

I am immensely grateful for the academic mentors who have guided me to where I am today. I am thankful for the late Patricia Latessa, my High School AP Psychology teacher, who first introduced me to the study of psychology. I wish to thank Golnaz Tabibnia and Greg Siegle, my post-baccalaureate research supervisors, who inspired and motivated me to pursue graduate training in psychology and neuroscience. Finally, I wish to thank Pete Gianaros and Anna Marsland, my graduate program co-mentors, for their kindness, unwavering support, and boundless generosity. I will always cherish your mentorship, and I promise to "pay it forward" to others.

I would also like to thank the students and staff in the Behavioral Neurophysiology Lab, including Annie Ginty, Dora Kuan, Gina Leckie, Kimberly Lockwood, Jenn MacCormack, Mark Scudder, Lei Sheu, Sara Snyder, and Chrystal Spencer - you have made graduate school a lot of fun. A special shout-out to my Bio-Health cohort pals, Caitlin DuPont and Jamie Peven, for always being available to commiserate as we progressed through the program together.

I would like to thank the members of my dissertation committee, who provided incredibly helpful feedback on the proposed research and guided it in a positive direction.

Finally, I wish to thank my family. To Mom and Dad, Alina, and Johanna: thank you for always supporting me. And to my husband, Jon: thank you for always believing in me. Lastly, I am grateful for our two cats, Gary and Gracie, for being the best stress relievers.

# 1.0 Introduction

## 1.1 Stressor-evoked cardiovascular reactivity: behavioral and health significance

Stress is ubiquitous in life. A stressor can be defined as an environmental, situational, or life event stimulus that may be appraised by an individual as taxing or exceeding their ability to cope with or respond adequately to it (Kivimäki & Kawachi, 2015; Lee et al., 2003). Stressors may take the form of external stimuli perceived by the individual (e.g., an argument or traffic jam) or internally generated thoughts and cognitions (e.g., recalling a past traumatic experience, anticipating a future event). Whether a stimulus is categorized by an individual as a stressor depends on external factors such as the intensity, duration, predictability, and controllability of the stressor, as well as internal factors such as an individual's history, goals, and expectations (Cohen et al., 2016). Psychological perspectives on acute stress posit that encounters with stressors engage primary appraisals, in which an individual interprets the stressor in order to gauge the level of threat, personal relevance, and meaning, as well as secondary appraisals, in which an individual estimates whether they have sufficient resources to adequately engage or cope with the stressor (Folkman, Lazarus, Gruen, et al., 1986). Hence, according to the above perspectives, stressors or demands that are appraised as exceeding the ability to cope will result in subjective experiences of "stress" (Folkman, Lazarus, Dunkel-Schetter, et al., 1986). In conclusion, both primary and secondary psychological appraisals are implicated in translating stressor exposure to the subjective experience of psychological stress.

In addition to evoking psychological experiences of stress, acute stressful experiences elicit changes in cardiovascular, neuroendocrine, and immune physiology. From a biological

perspective, these physiological changes may be adaptive insofar as they prepare an organism to behaviorally respond to the experience (Weiner, 1992). More specifically and in the context of cardiovascular physiology, changes evoked by psychological threats are functionally implicated in the recruitment and redirection of metabolic support towards peripheral muscles and tissues that are needed in order to engage with (or flee from) threats in the environment (Carroll et al., 2009; Obrist, 1981). Historically, these cardiovascular changes were once described as "defense reactions" (Hess & Brügger, 1943) and are henceforth termed *stressor-evoked cardiovascular reactivity*.

Two well-studied metrics of stressor-evoked cardiovascular reactivity include heart rate (HR) and blood pressure (BP). Both HR and BP, as well as other endpoints of cardiovascular physiology, are determined by complex autonomic, humoral, endocrine, and immune processes (Gordan et al., 2015; Hall, 2015). Heart rate refers to the number of heart beats measured within a time period (usually expressed in beats per minute) and is reciprocal to the heart period, which refers to the length of time in between heart beats (usually expressed in milliseconds). In contrast, BP refers to the pressure of circulating blood against arterial walls in the vasculature, and therefore is determined by both cardiac (e.g., HR) as well as vascular (e.g., peripheral resistance) factors. A chief mechanism governing top-down control of the heart and vasculature is via the two arms of the autonomic nervous system (ANS); namely the sympathetic nervous system (SNS) and parasympathetic nervous system (PNS). To elaborate, HR is chiefly determined by intrinsic "pacemaker" cells in the sinoatrial (SA) node of the heart, which spontaneously depolarize in order to initiate contraction. These pacemaker cells and their firing patterns are primarily under tonic inhibitory control by PNS activity via vagal cholinergic pathways. In addition, SNS-mediated beta-adrenergic input both lowers the threshold for excitation of SA node cells and increases myocardial

contractility, resulting in increased cardiac output. Finally, SNS outflow activates alpha-adrenergic receptors in peripheral vessels, which increases vascular resistance and therefore increases BP. Accordingly, as BP is substantially influenced by HR, the two metrics tend to be moderately correlated across individuals and behavioral contexts (Hall, 2015).

During acute stressful experiences, both BP and HR tend to rise (McEwen, 1998), and this change is primarily mediated via increased and decreased activity in the sympathetic and parasympathetic branches of the autonomic nervous system (ANS), respectively (Grossman et al., 1996; Mills & Dimsdale, 1991). However, while stressors tend to increase SNS and decrease PNS activity, the patterning of these branches are not universally reciprocal in nature, and can sometimes act in independent or coactive patterns (Allen & Crowell, 1989; Berntson et al., 1994; Brindle et al., 2014). Specifically, while BP and HR each comprise multiply determined end points of physiology, their stressor-evoked changes are generally thought to be mediated via some combination of beta-adrenergic sympathetic activation as well as vagal parasympathetic withdrawal, both of which tends to vary across individuals and across behavioral states (Berntson & Cacioppo, 2007). Hence, HR and BP are not "biomarkers" or indicators or either SNS or PNS activity per se, but rather reflect a complex combination of the latter two ANS branches, which therefore suggests they may be governed by separable neural systems higher in the brain.

Stressor-evoked cardiovascular reactivity has garnered the interest of health psychology and behavioral medicine researchers due to its speculated link to health outcomes. To elaborate, individuals vary appreciably in the magnitude and patterning of their cardiovascular reactions to stress, with some individuals exhibiting large-scale, or exaggerated reactivity (Allen et al., 1991). Moreover, these individual differences appear to be reliable and stable across individuals and over time (Kamarck et al., 1992, 1994; Kasprowicz et al., 1990). Previously, these observations led to

the hypothesis that repeatedly exaggerated expression of stressor-evoked cardiovascular reactivity could confer risk for CVD (Krantz & Manuck, 1984). This hypothesis has been supported by experimental animal models of social primates, showing that cardiovascular reactivity to stress associates with the severity of atherosclerotic lesions (Manuck et al., 1983). Exaggerated cardiovascular reactivity also predicts CVD risk across several human studies (Gianaros et al., 2002; Jennings et al., 2004; Kamarck et al., 1997). Stressor-evoked cardiovascular reactivity may interact with stressful life experiences to predict CVD risk (Kamarck et al., 2018) which is consistent with a diathesis-stress model of health and disease, in which a stable trait (i.e., diathesis; here, a phenotype for reactivity) interacts with external stressors to confer the greatest risk. Mechanistically, large-magnitude cardiovascular reactions to stressors may relate to elevated CVD risk by promoting changes in vascular tissue that promote atherosclerosis, or the chronic thickening of the arterial wall (Treiber et al., 2003). These changes are mediated via several possible mechanisms, including increased patterns of turbulent blood flow within the vasculature, increased shear stress on the arterial walls, as well as disruptions to metabolism in epithelial cells (Bairey Merz et al., 2002). Systematic reviews and meta-analyses examining prospective associations between metrics of cardiovascular reactivity and physical health outcomes showed the strongest and most consistent effects for systolic blood pressure (SBP) reactivity, hence emphasizing its potential role for health (Chida & Steptoe, 2010; Turner et al., 2020). In contrast, HR reactivity does not tend to show consistent effects with future cardiovascular health across studies (Chida & Steptoe, 2010).

To conclude, individual differences in stressor-evoked cardiovascular reactivity may be linked to physical health outcomes; however, there is still an incomplete understanding of the mechanisms that may contribute this link. To this end, the brain is thought to comprise the key

pathway linking acute psychological stress with downstream cardiovascular reactivity and potential cardiovascular disease risk (Gianaros & Jennings, 2018; Gianaros & Wager, 2015; Kraynak et al., 2018).

**Brain imaging studies of stressor-evoked cardiovascular reactivity.** To examine the above knowledge gap, human brain imaging and psychophysiology research has examined the brain and physiological mechanisms thought to be implicated in generating and regulating stressor-evoked cardiovascular reactivity. To this end, studies administer standardized laboratory batteries that aim to recreate a conceptually valid experience of psychological stress in the brain imaging environment. To do so requires developing a protocol that incorporates enough of what are considered to be the key ingredients of a stressful experience, each involving a combination of processing conflicting or cognitively demanding stimuli, performing under time pressure and without certainty of success, and receiving negative feedback from the environment (Debski et al., 1991; Steptoe & Vögele, 1991). Examples of these tasks include completing difficult mental arithmetic tasks under time pressure or preparing to give a difficult speech before an audience. In these studies, participants perform acute stress tasks during brain imaging and concurrent peripheral cardiovascular recording. Brain imaging methods employed in these studies include positron emission tomography (PET) and functional magnetic resonance imaging (fMRI).

Early brain imaging studies on the neural correlates of stressor-evoked cardiovascular reactivity focused on correlations on a within-participant basis; namely, these studies examined the correspondence between changes in cardiovascular physiology across a session within each participant separately, and subsequently tested whether there were stable associations within the brain across participants. For example, in one of the first published brain imaging studies on this

topic, 6 participants underwent PET scanning while performing stressful mental arithmetic and handgrip tasks (Critchley et al., 2000). For each participant, a general linear model was constructed to test for the association between change in mean arterial pressure (MAP) and the PET response for individual 60-second periods of stressor tasks. The estimates from these general linear models were then combined at the group level to identify where these associations were consistent across individuals. Results from this study indicated that mean arterial pressure was correlated with PET response within the dorsal anterior cingulate cortex (dACC), cerebellum, and brainstem. This same within-participant approach has been applied in several other studies that used cognitive (Gianaros et al., 2004, 2005) and socioevaluative stress tasks (Fechir et al., 2010; Wager, van Ast, et al., 2009; Wager, Waugh, et al., 2009).

In contrast to the above studies testing at the within-participant level, several studies have examined neural correlates of stressor-evoked cardiovascular reactivity at the between-participant level. By taking an individual differences approach, these latter studies have identified regions where individual differences in stressor-evoked cardiovascular reactivity associate with stressor-evoked neural activity. Specifically, these brain imaging studies adopt a similar approach as standard laboratory psychophysiology studies, by calculating for each participant a change score in cardiovascular physiology from baseline or a non-stress condition and calculating a corresponding map of BOLD response from the corresponding brain imaging data. For example, individual differences in SBP responses to a cognitive stressor paradigm were associated with corresponding individual differences in task-evoked activity in the perigenual ACC (pgACC) and amygdala (Gianaros et al., 2008).

While between-participant and within-participant approaches as described above may appear similar, it can be argued that they may provide complementary information about stress,

the brain, and cardiovascular control. More specifically, as discussed above, individual differences in stressor-evoked cardiovascular reactivity are more likely to reveal neural correlates that reflect stable and trait-like phenotypes, which may emerge from a combination of genetic, developmental, psychosocial, and other influences (Wu et al., 2010). As such, studies of individual differences in reactivity sometimes consider these competing factors by statistically covarying for them. In contrast, within-participant approaches might reveal neural correlates that more closely reflect processes related to peripheral physiological control that are generalizable across individuals. Put differently, between-participant approaches can plausibly inform individual phenotypes and risk factors, whereas within-participant approaches can plausibly inform psychological and physiology processes relevant to stress and health.

By examining associations between peripheral cardiovascular physiology and brain imaging metrics of neuronal activity, these studies have identified some of the brain systems that are implicated in stressor-evoked cardiovascular reactivity. To summarize, these studies point to a collection of brain regions and systems that include the medial prefrontal cortex (mPFC), anterior cingulate cortex (ACC), insula, amygdala, thalamus, and brainstem cell groups (Gianaros & Wager, 2015). Below I briefly review some of the findings on these brain systems and their speculated role in stressor-evoked cardiovascular reactivity.

### 1.2 Neurobiology of stressor-evoked cardiovascular reactivity

**mPFC and ACC.** The medial surface of the prefrontal lobe, comprising the medial prefrontal cortex (mPFC) and anterior cingulate cortex (ACC), is broadly linked to various cognitive, affective, and physiological processes relevant to stress and cardiovascular control. In

particular, the ventromedial subdivision of the PFC (vmPFC) is implicated in ascribing personal relevance to experiences and events, and generating so-called "affective meaning" (Roy et al., 2012), which is important for constructing psychological stress responses (Cohen et al., 2016). Moreover, the vmPFC is implicated in regulating PNS contributions to HR and BP (Thayer et al., 2012; Thayer & Lane, 2009). In contrast, more dorsal regions of the mPFC and ACC are implicated in conflict monitoring, motivation, and error detection, which comprise separable components of stressor processing (Amiez & Procyk, 2019; Botvinick et al., 2004). Hence, different subdivisions of the mPFC and ACC may contribute to separable psychological components of stressful experiences. Similarly, with respect to cardiovascular physiology, mPFC and ACC control of the SNS and PNS arms of the ANS may be somatotopically organized, with more dorsal subdivisions of the mPFC and ACC more closely linked to pro-sympathetic and anti-parasympathetic control, and more ventral subdivisions linked to anti-sympathetic and pro-parasympathetic control (Critchley, 2004; Gianaros & Wager, 2015; Kraynak et al., in prep).

**Insula.** Like the mPFC and ACC, the insula is implicated in both psychological and physiological processes of stress and cardiovascular control. The insula processes viscerosensory information from internal organs and tissues - a process termed interoception (Craig, 2009; Khalsa et al., 2018) – which is important for maintaining homeostasis across behavioral states and contexts. Moreover, insula-mediated interoceptive processes are thought to play a role in how bodily states contribute to the construction of affective feelings, which likely contribute to subjective experiences of psychological stress (Damasio & Carvalho, 2013). Moreover, the insula regulates cardiac function and is implicated in stress-related cardiac disorder and dysfunction, in particular stress-related cardiac arrhythmias (S. Oppenheimer & Cechetto, 2016; S. M. Oppenheimer et al., 1991).

**Amygdala.** The amygdala has long been implicated in processing salient stimuli, particularly those that involve threat and unpredictability (Davis & Whalen, 2001; LeDoux, 2003; Lindquist et al., 2016). Moreover, the amygdala is implicated in stress-related HR and BP responses to emotional contexts (Goldstein et al., 1996), although the consistency of the size and direction of these effects are unresolved (Gianaros et al., 2008, 2020).

As a part of my comprehensive exam project, I reviewed and meta-analytically synthesized the above literature on the neural correlates of stressor-evoked cardiovascular reactivity (Kraynak et al., in prep). This meta-analysis revealed that across 11 studies of stressor-evoked cardiovascular reactivity, there were consistent effects in clusters in the medial prefrontal cortex (PFC), including the ventromedial PFC and dACC, as well as the insula, thalamus, amygdala, and putamen, consistent with prior meta-analyses (Beissner et al., 2013; Gianaros & Sheu, 2009; Ruiz Vargas et al., 2016). Importantly, ancillary analyses from this meta-analysis suggested that studies utilizing within-participant designs reported more consistent effects than studies utilizing between-subject designs in the ACC, vmPFC, insula, amygdala, and thalamus (Kraynak et al., in prep). To conclude, there is accumulating evidence that brain activity in these brain regions is associated with stressor-evoked cardiovascular reactivity, in line with the view that these regions may be engaged by psychological stressors and may regulate internal physiology.

### 1.3 Multivariate brain imaging signatures of stress and cardiovascular reactivity

Importantly, most the above imaging studies of stressor-evoked cardiovascular reactivity have several limitations and shortcomings, many of which can be attributable to how these studies build statistical models with their brain imaging and psychophysiology data. More concretely,

most of the above studies use mass univariate statistical testing, which entails constructing and estimating separate general linear models (GLMs) for every voxel in the brain, resulting in several hundred thousand statistical models which are individually constructed and estimated. Subsequently, thresholds are applied to these thousands of voxels to identify the voxels or groups of voxels (i.e., clusters) that exhibit the most significant effects (Benjamini & Hochberg, 1995).

Indeed, the above mass-univariate approach produces at least 4 potential limitations. First, because these mass univariate approaches employ multiple statistical tests across thousands of voxels in the brain, extreme associations may be highlighted, resulting in an elevated false positive rate (Eklund et al., 2016; Kriegeskorte et al., 2009; Vul et al., 2009). Moreover, due to multiple testing, only highly significant associations are revealed, which in turn may produce statistical *false negatives* when testing on small samples or data with few observations (Marek et al., 2020). Second, from a psychometric perspective, the test reliability of BOLD responses in individual voxels tends to be poor, which severely limits its ability to identify correlates of behavior and physiology that are reliable across observations and contexts (Elliott et al., 2020). Third, the regression models employed in many of these mass univariate approaches treats the behavioral metric of interest as the predictor (X) and BOLD response in the brain as the outcome (Y), whereas in the context of stressor-evoked cardiovascular reactivity, this conceptual equation may be reversed. Fourth, the statistical models produced by this approach are purely descriptive in nature, and therefore are not used to generalize to predict outcomes (e.g., reactivity) in independent observations and individuals.

The above issues were particularly apparent with respect to literature bearing on the neural correlates of stressor-evoked cardiovascular reactivity, as revealed by meta-analytic findings from my comprehensive exam project. Specifically, whereas the studies of stressor-evoked

cardiovascular reactivity reported effects in the brain that appeared to be "consistent" across studies when applying cluster-based statistical thresholding, the average proportion of studies reporting "consistent" effects in these regions was 0.52 (max 0.69). This suggests that overall reproducibility of these findings in the brain is only moderate in magnitude (Kraynak et al., in prep). Thus, in order to identify reliable, reproducible, and generalizable neural correlates of stressor-evoked cardiovascular reactivity, more sophisticated approaches may be needed.

Accordingly, approaches combining dimensionality reduction, machine learning, and cross-validation techniques may address each of the above limitations (Coutanche & Hallion, 2019; Haxby et al., 2001; Woo et al., 2017). First, given the large number of variables (features) in the BOLD response, such that the number of predictive features (i.e., voxels of BOLD response) tends to vastly exceed the number of observations (i.e., trials, conditions, or participants), dimensionality reduction approaches such as principal component analysis can simplify the representation of the BOLD response into higher-order components, similar to how factor analyses identify higher-order latent factors of complex sets of features. Cross-validation is used to train models in one dataset and apply that model towards unseen observations and individuals. In the context of multivariate brain imaging models, cross-validation is used both to evaluate the stability of the model as well as its generalizability to novel contexts and participant samples.

The above approaches are thus focused on understanding how patterns of brain activity reliably predict behavior, as opposed to the traditional mass-univariate "brain mapping" approaches that examine associations without respect to overall patterns. Importantly, as mentioned above, machine-learning approaches produce testable models, or *signatures,* of brain activity that can then be applied to novel samples, behavioral contexts, and psychological processes. This in turn produces a powerful framework for testing for generalizable signatures of

stress and stressor-evoked cardiovascular reactivity. One salient example of this line of inquiry has been progressing in research on the neural correlates of pain processing. Here, a multivariate signature of thermal pain processing, termed the Neurologic Pain Signature (Wager et al., 2013), has been applied to test its sensitivity, specificity, and generalizability toward characterizing pain processing across various contexts related to thermal pain, including observed pain (Krishnan et al., 2016), social pain (Woo et al., 2014), and cognitive regulation of pain (Woo et al., 2015), among others.

In the context of stressor-evoked cardiovascular reactivity, this line of inquiry can be powerfully applied to test questions such as: Are the multivariate brain signatures of one metric of cardiovascular physiology (e.g., HR reactivity) specific to only that metric, or are they generalizable to another metric (e.g., SBP reactivity)? Do multivariate signatures of reactivity to one type of psychological stress task (e.g., speech preparation) generalize to reactivity to another type (e.g., difficult cognitive challenges)? Are multivariate signatures of reactivity in a healthy college sample generalizable to midlife adults with or without subclinical cardiovascular disease or other comorbid conditions? These questions may be key to developing a cumulative and generative science on the neural correlates of stressor-evoked cardiovascular reactivity, yet more studies are needed in order to contribute towards developing a repertoire of brain signatures across various stress tasks, samples, and outcomes.

Indeed, to my knowledge, only two studies have used the above machine learning and cross-validation techniques to identify multivariate signatures of brain activity that predict cardiovascular reactivity to psychological stress. As detailed below, these two studies share several commonalities in their approaches and findings, yet nonetheless have several important

differences. As the proposed dissertation project aims to fill critical gaps in knowledge revealed by these two studies, both studies are detailed below.

The first of these two studies examined multivariate predictors of HR reactivity on a within-participant basis to a socioevaluative stress task (Eisenbarth et al., 2016). In this study, 18 college-aged healthy participants underwent a so-called "speech preparation" socioevaluative stress paradigm, in which they were instructed to prepare themselves to give a speech before a panel of professors and experts. The speech preparation task involved 2 separate 2-minute periods of speech preparation. Participants did not end up being asked to administer the speech; however, the speech preparation period reliably altered heart rate (HR) and skin conductance level (SCL), another measure of ANS activity. This study successfully developed two whole-brain multivariate signatures that predicted within-participant changes in HR and SCL. The average correlation between predicted and observed HR across participants was $r$ = .54, whereas the average correlation between predicted and observed SCR was $r$ = .58. Significant weights for the HR signature were observed in the dACC, vmPFC, hippocampus, and temporal pole. The multivariate signatures predicting HR and SCL were only moderately correlated with each other, suggesting that different brain systems may be involved in regulating pathways of autonomic outflow to affect various end organ systems.

The second study examined multivariate predictors of SBP reactivity on a between-participant basis to two cognitive stress tasks (Gianaros et al., 2017). The cognitive stressor protocol comprised a color-word Stroop task and a Multisource Interference Task (MSIT), respectively (Bush & Shin, 2006). In contrast to the study by Eisenbarth et al., this study tested a community sample of midlife adults. This study successfully developed a whole-brain multivariate signature that predicted *individual differences* in SBP reactivity. Specifically, the correlation

between predicted and observed SBP reactivity was $r$ = .32 in a hold-out test sample. Significant weights for the SBP signature were observed in the dACC, vmPFC, insula, amygdala, basal ganglia, thalamus, and cerebellum, among others.

### 1.4 Interim summary and open questions

Taken together, the above brain imaging literature on the neural correlates of stressor-evoked cardiovascular reactivity stand to greatly improve our understanding of the brain bases of stress-related mechanisms underlying cardiovascular disease risk. However, the modest consistency of these findings raises important concerns about their reliability and replicability; hence, it is proposed to redress these concerns by implementing multivariate approaches, which incorporate dimensionality reduction, machine learning, and cross-validation, to identify signatures of brain activity and connectivity can predict changes in cardiovascular responses to stress. Yet, there is relatively little research implementing the above machine learning approaches in the context of stressor-evoked cardiovascular reactivity, and several open questions remain.

For instance, it is currently unclear to what extent the multivariate signature of HR reactivity developed by Eisenbarth et al. generalizes to predict HR evoked by other stressor paradigms, (e.g., cognitive challenges) or measured in different samples (e.g., midlife adults). This is an open question to the extent that different types of psychological stressors may evoke differing signatures of neural activity that nonetheless lead to relatively similar responses in cardiovascular output, or rather to the extent that the neural correlates of cardiovascular reactivity may vary across the lifespan. Similarly, it is unclear to what extent the multivariate signature of SBP reactivity identified in the study by Gianaros et al. (2017), focusing on individual differences in SBP

reactivity, generalizes to or shares commonalities with signatures that predict within-participant change over time, even in the same sample of participants. For example, it was recently shown that multivariate brain signatures predicting within-person changes in pain reports to thermal pain were comprised of different brain regions and networks than those predicting individual differences in overall pain reports in the same participants (Petre et al., 2019). Hence, these questions have the potential to deepen our understanding of the brain systems that may link stressful experiences to cardiovascular reactivity and potentially CVD risk, across stress contexts, participant samples, and endpoints of cardiovascular physiology.

To this end, the current study aimed to build off prior work by developing multivariate brain signatures of BP and HR reactivity, on a within-participant basis, to a cognitive stressor paradigm in a community sample of midlife adults. Thus, the current study primarily focused on SBP reactivity as its cardiovascular metric of interest, due to its relevance to health, but also examined HR reactivity, due to its prominence in the psychophysiology literature. In addition, the current study integrated these findings in the context of multivariate signatures developed and published elsewhere, and to test whether previously published signatures could predict reactivity in these data.

### 1.5 Study aims

Accordingly, to address these gaps, the current study had the following aims:

**Aim 1:** Using machine learning and cross-validation, develop whole-brain multivariate signatures of brain activity that predict within-participant variation in SBP and HR reactivity during a cognitive stressor paradigm. The goal was to theoretically replicate and extend the work by

Eisenbarth et al. (2016) in a novel sample comprising midlife adults (as opposed to young adults) with a cognitive challenge paradigm (as opposed to a socioevaluative stressor paradigm) and considering additional health-relevant metrics of cardiovascular physiology (i.e., SBP).

**Hypothesis 1a:** A multivariate signature of brain activity will predict changes in ***systolic blood pressure (SBP)*** during psychological stress. Whereas the signature will be whole-brain in nature, significant contributors to the signature will comprise core brain regions involved in stress and BP control, including the dACC, insula, amygdala, thalamus, PAG, and brainstem.

**Hypothesis 1b:** A multivariate signature of brain activity will predict changes in ***heart rate (HR)*** during psychological stress. Similar to the above, the signature will be whole-brain in nature, but significant contributors to the signature will comprise core brain regions involved in stress and HR control, including the vmPFC, insula, amygdala, thalamus, PAG, and brainstem.

**Hypothesis 1c:** Each of the two multivariate signatures identified above will generalize to significantly predict changes in the other metric of cardiovascular physiology. For example, the multivariate signature predicting SBP will generalize to predict significant variance in HR, and vice versa. However, the effect size of this prediction will be smaller in magnitude as compared to the prediction of its own measure of cardiovascular physiology (e.g., SBP), in line with the findings of Eisenbarth et al. (2016).

**Hypothesis 1d:** In addition to generalizing to the other metric of cardiovascular physiology, idiographic predictions at the group level will generalize to significantly predict reactivity in held-out individuals (i.e., group-based prediction). However, the effect size of this

prediction will be smaller in magnitude as compared to the idiographic predictions examined above, in line with the findings of Eisenbarth et al. (2016).

**Aim 2:** Examine the generalizability of previously published multivariate signatures of stressor-evoked cardiovascular reactivity as they relate to within-participant changes in BP and HR to these stressor paradigms. The goal of this aim was to situate the findings of Aim 1 in the context of prior literature and identify common and distinct features of these multivariate predictors of cardiovascular reactivity. Thus, the first hypothesis involved characterizing the similarities and differences between all multivariate signatures, whereas the latter hypotheses involved applying the previously published multivariate maps to the present data.

**Hypothesis 2a:** Multivariate signatures produced from the current study (Aim 1) will show several commonalities with prior maps, notably that they each comprise core visceral control areas.

**Hypothesis 2b:** The multivariate signature predicting individual differences in SBP reactivity to a cognitive stressor as reported by Gianaros et al. (2017) will not significantly predict within-person changes in SBP to the same cognitive stressor.

**Hypothesis 2c:** The multivariate signature predicting HR reactivity to a psychosocial stressor as reported by Eisenbarth et al. (2016) will not significantly predict changes in HR to a cognitive stressor.

# 2.0 Methods

## 2.1 Participants

Participants were drawn from the Pittsburgh Imaging Project (PIP), which is a longitudinal study of the psychosocial and neurophysiological correlates of CVD risk and its progression over midlife (Gianaros et al., 2017; Sheu et al., 2012). Participants in PIP were 331 midlife men (N = 165) and women (N = 166) aged 30 to 51 years old and were recruited between 2008 and 2014 via mass mailings to community residents in Southwestern Pennsylvania. Participants were free of chronic physical health conditions, including any history of clinical coronary heart disease or a cardiovascular disease event, cardiovascular surgery, cancer, chronic kidney or liver condition, type 1 or 2 diabetes mellitus, or pulmonary or respiratory disease (Gianaros et al., 2017). Participants also did not report any current or past psychiatric diagnoses of substance abuse disorders. All participants provided informed consent to participate in study protocols, and the study was approved by the University of Pittsburgh Institutional Review Board.

The present study was the first analysis on fMRI-based multivariate signatures of within-participant changes in stressor-evoked cardiovascular reactivity in the PIP sample; as mentioned above, a prior report examined multivariate predictors of individual differences in stressor-evoked cardiovascular reactivity in the same sample (Gianaros et al., 2017).

## 2.2 Procedures

### 2.2.1 MRI protocol

Data for the proposed study was drawn from the MRI assessment taken during the baseline wave of the PIP study. This MRI assessment started between 7:00 and 11:00 AM, and participants refrained from eating, exercising, and consuming caffeinated and tobacco products, as well as drinking alcoholic beverages, for at least 8 hours prior to the start of this visit. At the MRI assessment, participants underwent seated BP measurement and practiced the MRI stressor tasks with a trained research assistant. Participants were then inserted into the MRI scanner and rested for 20 minutes. During this time, 3 to 5 baseline prestressor BP and HR measurements were collected (see below). While in the scanner, participants then completed 2 stressor tasks during functional MRI (fMRI) acquisition and BP and HR monitoring (see below). A high resolution structural MPRAGE scan was acquired between the 2 stressor tasks.

### 2.2.2 Stressor protocol

The psychological stressor protocol as implemented in PIP included a color-word Stroop task (Boutcher & Boutcher, 2006) and a modified Multi-Source Interference Task (MSIT; Bush & Shin, 2006), each modified for the MRI scanner environment and each modified to induce a prototypical stressful experience (Sheu et al., 2012). Specifically, each task required participants to process conflicting information, perform under time pressure, and respond to negative feedback. Tasks were presented using ePrime 2.0 (Pittsburgh, PA).

In each task, participants completed 4 blocks of trials in an incongruent condition, which were each interleaved with 4 blocks of trials in a congruent condition. Each incongruent and congruent block lasted between 52 and 60 seconds and were preceded by a 10- to 17- second fixation (rest) period. Each task lasted 9 minutes 20 seconds.

In the color-word Stroop, participants were presented with a target word in the center of the screen along with four identifier words (red, blue, yellow, green) at the bottom of the screen. During all Stroop trials, participants were instructed to select the position of the identifier word at the bottom of the screen that named the text color of the target word. During Stroop congruent trials, the color of the target word matched the color of all the words at the bottom of the screen. During Stroop incongruent trials, all color words were mismatched with their text color. Separately, in the MSIT, three numbers (each 1 – 3) were presented on the screen, with two identical numbers and one differing number. In all MSIT trials, participants were instructed to identify the position of the differing number. During MSIT congruent trials, the value and the position of the differing number match, whereas during MSIT incongruent trials the value and position of the differing number did not match.

In both tasks, participants were instructed to respond using a button press fastened to their right hand (1=thumb, 2=index, 3=middle, 4=ring). Following their response, participants were provided positive (green checkmark) or negative (red x-mark) feedback based on their trial performance. To account for individual differences in behavioral performance, in both stressor tasks, incongruent trial periods were titrated to adjust the amount of time allowed for the participant to respond. This titration was implemented such that each participant would not surpass 60% overall accuracy during incongruent blocks. The titration was implemented by adjusting the amount of time the participant was allotted to respond; after 3 consecutive correct responses, this

time allotment was shortened by 300 milliseconds, and after 3 consecutive incorrect responses, this time allotment was lengthened by 300 milliseconds. If the participant failed to respond within the allotted time frame, they the computer would indicate they were too late.

Measures of trial response accuracy and reaction time were recorded by the ePrime software. These measures were averaged across trials within each condition (incongruent, congruent) to verify the tasks successfully titrated accuracy and reaction time. Measures of accuracy and reaction time were also averaged across trials within individual blocks for later analysis.

### 2.2.3 Cardiovascular monitoring

During MRI, BP and HR were measured during the resting (prestressor) and stressor task periods from the brachial artery of the left arm using an oscillometric device. Specifically, the device was set to inflate every 2.5 minutes during the prestressor period and once during each incongruent and congruent block of the Stroop and MSIT. The device reported 1 reading of HR, SBP, diastolic BP (DBP), and mean arterial pressure (MAP) per reading. Hence, in contrast to the continuous HR monitoring as implemented in Eisenbarth et al. (2016), 1 reading of BP and HR was collected per each incongruent and congruent block in the Stroop and MSIT, which is taken to reflect the overall ambient BP and HR during that period. Moreover, unlike the study by Eisenbarth et al. (2016), SCL was not collected. Accordingly, 3 to 5 baseline prestressor readings were collected for each participant, as well as 16 task-related readings in total (8 Stroop and 8 MSIT, each comprising 4 incongruent and 4 congruent readings).

## 2.3 Data analysis

### 2.3.1 Cardiovascular reactivity

For SBP and HR separately, reactivity scores were calculated for each task block by subtracting the average of the final 3 prestressor readings from the task block reading. Accordingly, a reactivity score of 0 mmHg or 0 BPM indicated no change in SBP or HR from the average of the baseline reading, respectively. For each participant, the distribution of these reactivity scores were visually inspected. Reactivity scores greater than 3 standard deviations from the mean were flagged and interpolated to the nearest neighbor. Various metrics of SBP and HR were examined, including the mean prestressor baseline reading, mean reactivity, standard deviation of reactivity, as well as mean reactivity separated by incongruent and congruent conditions during Stroop and MSIT.

### 2.3.2 MRI data acquisition

Functional MRI (fMRI) data were acquired on a 3 T Trio TIM whole-body MRI scanner (Siemens, Erlangen, Germany), equipped with a 12-channel phased-array head coil. Blood-oxygen level-dependent (BOLD) images were acquired with a gradient-echo EPI sequence using the following parameters: field-of-view (FOV) = 205 × 205 $mm^2$, matrix size = 64 × 64 $mm^2$, repetition time (TR) = 2,000 ms, echo time (TE) = 28 ms, and flip angle (FA) = 90. Thirty-nine slices (3 mm thickness, no gap) were obtained in an interleaved sequence in an inferior-to-superior direction, yielding 280 BOLD images per task. For spatial coregistration of BOLD images, $T_1$ weighted 3D magnetization-prepared rapid gradient echo (MPRAGE) neuroanatomical images

were acquired over 7 min 17s by these parameters: FOV = 256 × 208 $mm^2$, matrix size = 256 × 208 $mm^2$, TR = 2,100 ms, time-to-inversion (TI) = 1,100ms, TE = 3.29ms, and FA=8.

### 2.3.3 MRI preprocessing and first level analysis

BOLD fMRI data from the Stroop and MSIT were processed using Statistical Parametric Mapping (SPM) software, version 12 (SPM12; http://www.fil.ion.ucl.ac.uk/spm/). For each task, images were realigned to the first image, corrected for motion distortion, and normalized to Montreal Neurological Institute space. Normalized images were rescaled (2-mm isotropic voxels) and smoothed with a 6-mm full width at half maximum Gaussian kernel.

Prior reports using these data constructed individual first-level general linear models (GLM) and contrast maps to model the main effects of condition (Incongruent versus Congruent) for the Stroop and MSIT (Gianaros et al., 2017). The present study reports the results of these main effects contrast maps in the analytic sample (N = 242). Moreover, the present study constructed novel GLMs that accounted for block-specific patterns of brain activity. Specifically, in individual first-level analyses, a separate regressor modeled each of the 8 blocks of incongruent and congruent trials for each task. This approach is comparable to a so-called 'beta series' design, in which every trial is modeled separately in a design matrix (Rissman et al., 2004). Each block was therefore modeled using separate regressors, each convolved with a double gamma hemodynamic response function in SPM. Accordingly, individual first-level analysis GLMs produced 8 block-related whole-brain beta maps per task. Regressors corresponding to the presence of the incongruent versus congruent conditions were not modeled. Finally, regressors of no interest included the 6 realignment parameters derived from preprocessing, 2 timeseries reflecting the mean white matter and cerebrospinal fluid signal, as well as their temporal derivatives and square

terms of all 8 signals, yielding a total of 32 regressors of no interest (Ciric et al., 2017; Satterthwaite et al., 2019). These regressors of no interest were included in all GLMs to account for motion and physiological artifacts that may influence the BOLD signal (Power et al., 2013, 2015).

### 2.4 Aim 1: Multivariate signature development

Several algorithms exist for multivariate and machine learning approaches to brain imaging data, including support vector regression (SVR), principal components regression (PCR), least absolute shrinkage and selection operator (LASSO) regression, ridge regression, elastic net regression, decision trees, and more (Hastie et al., 2009). Each of these algorithms have different strengths and limitations as it pertains to multivariate analysis handling brain imaging data, which comprises large numbers of predictors which are moderately intercorrelated. The proposed study aims to use principal component regression combined with least absolute shrinkage and selection operator (hereafter, LASSO-PCR; Wager et al., 2011, 2013).

To clarify, by using a multivariate and machine learning framework, the BOLD responses as measured by the beta maps produced above, restricting within gray matter voxels, served as the multivariate predictor variable, and either SBP or HR reactivity served as the outcome variable. In line with the approach taken by Eisenbarth et al. (2016) the multivariate signatures were be used to make predictions about cardiovascular reactivity within individuals (idiographic cross-validation) and about new individuals (group-based cross-validation) (Eisenbarth et al., 2016).

The LASSO-PCR approach has been previously described in detail (Eisenbarth et al., 2016; Gianaros et al., 2017, 2020; Wager et al., 2011, 2013). In general, this approach combines dimensionality reduction (PCR) with penalized regression (LASSO) within a cross-validated

framework. More concretely, to reduce the dimensionality of the predictor variables (i.e., voxels in each block-related beta map), the voxel-by-block matrix were first submitted to a principal component analysis (PCA) using singular value decomposition (SVD). The outcome variable of interest (here, either SBP reactivity or HR reactivity) was then regressed onto the remaining principal components by LASSO regression using the 'lassoglm' function in MATLAB (Hastie et al., 2009; Tibshirani, 1996). In LASSO regression, beta coefficient estimation is subject to the L1 penalty (regularization), which selects predictive features by penalizing (shrinking) non-significant predictive features to zero (Efron et al., 2004; Zhao et al., 2009). The extent of this penalization procedure was constrained by the parameter lambda (λ), in which a higher λ produces a more penalized and thereby sparser predictor space. In the LASSO-PCR procedure, following this feature selection step, the sparse regression coefficient matrix was subsequently back-projected to voxel space via the SVD transformation matrix to produce a whole-brain weight map. Accordingly, the dot product of the whole-brain weight map with an individual contrast map was estimated to generate a predicted estimate of SBP or HR reactivity.

In line with the approach of Eisenbarth et al. (2016), primary analyses implemented idiographic cross-validation to develop individualized multivariate signatures of SBP and HR. As mentioned above, the shrinkage parameter λ described above determines the sparsity of regression models, and the influence of a given λ value is likely to differ according to input data. To this end, the λ parameter was optimized first using leave-one-out-cross-validation (LOOCV) in an 'inner loop' and applied in an 'outer loop' to predict individual reactivity observations using LOOCV again. LOOCV is a form of k-fold cross validation in which one observation serves as the test sample, and all other observations serve as the training sample. That is, to first identify the optimal shrinkage parameter, λ, and thus the number of principal components that best predict SBP (or

HR), LOOCV was applied within an inner loop, before generalizing to new observations in an outer loop. As such, the cross-validation approach employed here implemented "nested" cross validation. Within each cross-validation fold, LASSO-PCR was conducted on training samples using a sequence of 1000 λ values, and the performance of each λ was evaluated by calculating the average of the mean squared error (MSE) between predicted and observed reactivity in the testing sample. After identifying the optimal λ, the entire LASSO-PCR procedure was repeated using this λ on the entire inner loop sample, producing a whole-brain multivariate predictive pattern of cardiovascular reactivity.

The predictive performance of each multivariate signature was summarized using 4 types of statistics (5 metrics in total) describing either the association or the discrepancy between predicted and observed SBP and HR reactivity (Forman & Scholz, 2010), in line with prior work (Gianaros et al., 2020). Metrics were computed individually for each participant, and the descriptive statistics of metrics across the entire analytic sample was summarized using the mean and standard error (SE). First, the association between predicted and observed SBP and HR was characterized using the Spearman's rank correlation coefficient (*rho*). The nonparametric Spearman's rank correlation was chosen over the parametric Pearson correlation (r) in order to reduce the potential influence of outlier points, especially as the subject-specific predicted-observed associations were drawn from a small number of observations (i.e., 16 block-related reactivity observations per subject). A one-sample t-test was conducted on the entire group of predicted-observed *rho* values to test if idiographic model performance was significantly different from zero across individuals. Second, the discrepancy between predicted and observed reactivity was described using mean absolute error (MAE). Third, the variance in observed values explained by predicted values ($R^2$) was calculated using the sums of squares formulation (Poldrack et al.,

2020; Scheinost et al., 2019). Finally, Bayes Factors (BF10 and BF01) were used to describe the strength of the association between the predicted and observed reactivity and to aid in interpreting results that did not meet conventional statistical significance (Morey & Rouder, 2011). BF10 refers to the probability of the alternative hypothesis, relative to the null hypothesis, whereas BF01 refers to the probability of null hypothesis, relative to the alternative hypothesis.

To identify voxels that reliably contributed to a given brain signature of cardiovascular reactivity (i.e., SBP or HR), the respective multivariate signatures were combined across all participants, and a one-sample t-test was computed at each voxel. These t-statistic maps were thresholded using the false discovery rate [$q < 0.05$; (Benjamini & Hochberg, 1995)], in line with the approach of Eisenbarth et al (2016). Descriptive statistics of each cluster was reported in tables, including its size (number of voxels), center coordinates, and constituent brain regions. Moreover, the spatial similarity of the SBP and HR maps was compared by calculating the correlation across signatures for each participant and summarized for the analytic sample using the mean ± SE.

### 2.4.1 Cross-modality and group-based cross-validation

In addition to the above idiographic approach, the generalizability of each signature was examined both across physiological modality (i.e., SBP versus HR) and across participants. First, generalizability across physiological modality (within participants) was examined by applying each participant's brain signature corresponding to one measure (e.g., SBP) to their series of beta maps, and comparing predicted scores to observed scores of the other measure (e.g., HR), and vice versa. Second, generalizability across participants was examined by implementing 10-fold cross validation at the group level. That is, within each cross-validation loop, the multivariate signatures derived at the idiographic stage were averaged across training participants and applied to holdout

test participant beta maps. Importantly, the cross-validation fold membership was determined by stratifying across the respective mean reactivity scores (i.e., mean stressor-evoked SBP or HR reactivity). Model performance of cross-participant generalizability was examined using the same metrics as idiographic models. Finally, these 2 tests of generalizability were assessed by directly comparing model performance metrics to the primary, idiographic, within-modality approach, using paired t-tests (Eisenbarth et al. 2016).

### 2.5 Aim 2: Generalizability of published multivariate signatures

The multivariate signature for within-participant HR reactivity developed by Eisenbarth et al. (2016) was retrieved from the CANlab GitHub repository[1] and the multivariate signature for between-participant SBP reactivity developed by Gianaros et al. (2017) was retrieved from the CoAxLab GitHub repository[2]. For each participant and signature, the PIP Stroop and MSIT images were resampled to the signature image and cosine similarity was computed for each of the 16 block-related contrast maps to produce predicted observations of HR and SBP reactivity. The overall performance of these published signatures on PIP data was assessed using the same metrics as described above (Spearman's *rho*, $R^2$, MAE, Bayes Factors). These metrics were compared to the performance metrics of the multivariate signatures developed in Aim 1 using paired t-tests.

---

[1] https://github.com/canlab/Neuroimaging_Pattern_Masks/tree/master/Multivariate_signature_patterns/2016_Eisenbarth_JNeuro_autonomic_patterns

[2] https://github.com/CoAxLab/BPReactivityPhenotype

## 2.6 Planned supplementary analyses

### 2.6.1 Local spatial similarity analyses and network similarity analyses of signatures

In addition to testing the correspondence between SBP and HR signatures on a voxel-wise basis as described in Aim 1, additional analyses examined the correspondence between these signatures in terms of local patterns of prediction weights. Specifically, using a spherical searchlight with a 5 voxel radius, the spatial correlation between each participant's SBP and HR signature was calculated for each voxel's neighborhood, followed by a one-sample t-test to identify voxels where local patterns ere similar between signatures across participants (Eisenbarth et al., 2016). A second set of supplementary analyses examined the spatial correspondence of the idiographic SBP and HR signatures respect to established intrinsic networks (Yeo et al., 2011) consistent with prior work (Gianaros et al., 2020; Ginty et al., 2019). Specifically, the cosine similarity of the SBP and HR idiographic signatures (as well as their difference) was computed for 7 intrinsic networks (visual, somatomotor, dorsal attention, ventral attention, limbic, frontoparietal, default mode). The overall correspondence of each multivariate signature and their difference was evaluated using t-tests.

### 2.6.2 Psychometric properties of brain signatures

Psychometric properties of brain imaging data, such as test-retest reliability and internal consistency, may influence their predictive performance (Kragel et al., 2021). To explore this, the internal consistency of the Stroop and MSIT was calculated using the split-half method (Infantolino et al., 2018). Specifically, for each participant and task, general linear models were

constructed separately on the first and second half of the BOLD signal data, respectively. From these general linear models, voxel-wise contrasts reflecting the difference in BOLD signal during incongruent vs congruent conditions were computed. The internal consistency of each task was then computed by calculating the correlation between the contrast maps from the first and second halves of each task and applying the Spearman-Brown (SB) correction [$SB = 2r/(1+r)$]. Maps of internal consistency were thresholded according to standard conventions depicting 'fair,' 'good,' and 'excellent' reliability (Cicchetti, 1994). Finally, internal consistency maps were then averaged across tasks for each participant and compared on a voxel-wise basis to whole-brain main effects maps and signatures generated by the idiographic machine learning methods (Gianaros et al., 2020).

### 2.6.3 Contribution of nuisance variables

The BOLD signal may be sensitive hemodynamic coupling, which may vary as a function of cardiovascular arousal. Thus, it cannot be ruled out whether BOLD signal predictors of cardiovascular reactivity reflect true stressor-evoked "neural" changes. Moreover, excessive head motion significantly influences the BOLD signal and therefore may confound relationships between BOLD activity and within-participant changes in behavior (Power et al., 2012; Satterthwaite et al., 2013). Two sensitivity tests were conducted to examine these possibilities. First, the prediction of reactivity from pulsatile white matter and CSF nuisance signal was tested using idiographic LASSO-PCR. Second, the prediction of reactivity from the above nuisance components and motion covariates was tested using idiographic LASSO-PCR. In both analyses, block-related averages of nuisance variables (WM/CSF/motion) were computed to be used in

prediction analyses. Model performance for the prediction of cardiovascular reactivity from these nuisance variables was computed and reported as in Aim 1.

### 2.6.4 Predicting behavior from brain signatures of cardiovascular reactivity

In addition to testing the cross-modal (e.g., SBP vs HR, prior studies vs present study) generalizability of brain signatures, it is unclear whether these signatures would generalize to predict other behavioral or psychological outcomes related to the Stroop and MSIT. Measures of accuracy and reaction time were recorded in the Stroop and MSIT, and these variables were averaged within blocks. To this end, associations between ongoing behavioral performance and cardiovascular reactivity were explored. Moreover, it was tested whether signatures derived in Aim 1 generalized to predict behavioral performance.

## 2.7 Post-hoc exploratory analyses

Results of the Aim 1 analyses revealed that, for many participants, the LASSO-PCR algorithm did not generate reliable idiographic models of neither SBP nor HR reactivity (see Results Section 3.4). More concretely, for a large proportion of idiographic models (19% SBP models, 16.5% HR models), the optimized LASSO regularization parameter $\lambda$ returned zero components, thus producing a so-called 'null' model comprising a constant term and zero voxel weights. For these idiographic models, the model performance was uniformly poor (i.e., *negative* predicted-observed Spearman's *rho*'s). Given these null findings with respect to the primary aims of this study, two sets of post-hoc, unplanned exploratory analyses were conducted to further

identify the source of poor model performance. Specifically, the first set of post-hoc analyses examined sources of poor model performance across individuals, and the second set of post-hoc analyses explored alternative machine learning algorithms that may have been better suited to these data.

### 2.7.1 Examining sources of poor model performance

Various factors were explored that may have contributed to individual differences in the success of the LASSO-PCR algorithm to generate reliable models of stressor-evoked cardiovascular reactivity; these included resting cardiovascular physiology, mean cardiovascular reactivity, variability in cardiovascular reactivity, head motion, and behavioral performance. On these factors, participates for whom the LASSO-PCR generated so-called 'null' models were compared to participants for whom the LASSO-PCR model produced models comprising whole-brain weight maps. In addition, associations between each of these factors with a continuous measure of model performance (i.e., Spearman's *rho*) was assessed using multiple linear regression.

### 2.7.2 Exploring alternative machine learning approaches

Moreover, in view of the null findings bearing on idiographic models of cardiovascular reactivity, alternative machine learning approaches were explored. To elaborate, the above patterning of poor model performance may have been partially attributable to the sparsity constraint introduced by the LASSO shrinkage parameter, $\lambda$. To this end, other machine learning approaches that do not impose this shrinkage parameter may be more effective at reliably

generating models of cardiovascular reactivity, especially when the model comprises few predictors. Specifically, principal component regression (PCR) retains dimensionality reduction as in LASSO-PCR but does not apply regularization, thus avoiding the patterning of so-called 'null' models observed by LASSO-PCR. To this end, unplanned post-hoc analyses repeated the procedures described in Aim 1, replacing the LASSO-PCR algorithm with PCR. The model performance metrics were computed and reported as in Aim 1. Moreover, these post-hoc analyses were compared to the primary analyses reported in Aim 1 in terms of both model performance metrics as well as the multivariate patterns of BOLD activity.

### 2.8 Software and code availability

Analyses were conducted in the MATLAB environment using code previously developed for multivariate analysis of fMRI data (https://github.com/canlab) and in line with prior publications (Gianaros et al., 2020). Analysis code is available on GitHub (https://github.com/tekraynak/dissertation) and whole-brain maps are available on NeuroVault (https://neurovault.org/collections/HXXJSDEL) (Gorgolewski et al., 2015).

# 3.0 Results

## 3.1 Descriptive statistics

After quality control review of the complete PIP sample (N= 331), several participants were excluded for the following reasons: later endorsing antihypertensive medication use following MRI assessments (N = 1); poor behavioral compliance with stressor tasks (i.e., accuracy lower than chance on congruent trials; N = 2); MRI data acquisition or reconstruction failure (N = 8); insufficient BOLD signal coverage (N = 3); incompletely acquired cardiovascular monitoring (N = 75). Thus, analyses were conducted on an analytic sample of 242 participants (118 men, 124 women).

Participants excluded from analysis for the above reasons were compared to participants in the analytic sample according to primary study variables. Compared to excluded participants, included participants were younger ($t$ = -3.16 $p$ = .001), had lower BMI ($t$ = -4.29 $p$ < .001), had lower resting (pre-task) SBP ($t$ = -3.03 $p$ = .003), and exhibited less variability in stressor-evoked SBP ($t$ = -3.62 $p$ < .001). In contrast, included participants did not significantly differ from excluded participants in terms of sex, race, years of education, smoking status, task accuracy, task reaction time, resting HR, mean stressor-evoked SBP, mean stressor-evoked HR, and variability in stressor-evoked HR. Table 1 provides descriptive statistics of the analytic sample (N = 242).

**Table 1. Descriptive statistics of analytic sample.**

| **Characteristic (N = 242)** | **M ± SD or N (%)** |
|---|---|
| Age | 39.7 ± 6.21 |
| Sex | |
| Male | 118 (48.8%) |
| Female | 124 (51.2%) |
| Race and Ethnicity | |
| White | 172 (71.1%) |
| Black / African American | 54 (22.3%) |
| Asian | 13 (5.4%) |
| Multiracial | 2 (0.8%) |
| Other | 1 (0.4%) |
| Smoking Status | |
| Never | 148 (61.2%) |
| Former | 53 (21.9%) |
| Current | 41 (16.9%) |
| Years of School | 16.80 ± 3.26 |
| Body Mass Index | 26.10 ± 4.28 |
| *Cardiovascular physiology* | |
| SBP: baseline (mm Hg) | 122.00 ± 11.60 |
| SBP: stressor-evoked change (overall) (mm Hg) | 3.75 ± 5.11 |
| SBP: stressor-evoked standard deviation (overall) (mm Hg) | 4.22 ± 1.55 |
| SBP: stressor-evoked change (Stroop) (mm Hg) | 4.46 ± 5.94 |
| SBP: stressor-evoked standard deviation (Stroop) (mm Hg) | 3.87 ± 1.69 |
| SBP: stressor-evoked change (MSIT) (mm Hg) | 3.04 ± 4.79 |
| SBP: stressor-evoked standard deviation (MSIT) (mm Hg) | 3.83 ± 1.63 |
| HR: baseline (BPM) | 67.40 ± 9.23 |
| HR: stressor-evoked change (overall) (BPM) | 6.27 ± 4.87 |
| HR: stressor-evoked standard deviation (overall) (BPM) | 3.47 ± 1.84 |
| HR: stressor-evoked change (Stroop) (BPM) | 7.16 ± 5.70 |
| HR: stressor-evoked standard deviation (Stroop) (BPM) | 3.20 ± 1.85 |
| HR: stressor-evoked change (MSIT) (BPM) | 5.37 ± 4.65 |
| HR: stressor-evoked standard deviation (MSIT) (BPM) | 2.80 ± 1.48 |
| *Behavioral Performance* | |
| Mean accuracy, Stroop incongruent trials | 0.56 ± 0.09 |
| Mean accuracy, MSIT incongruent trials | 0.56 ± 0.09 |
| Mean accuracy, Stroop congruent trials | 0.84 ± 0.09 |
| Mean accuracy, MSIT congruent trials | 0.91 ± 0.07 |
| Mean reaction time, Stroop incongruent trials (sec) | 1.87 ± 0.50 |
| Mean reaction time, MSIT incongruent trials (sec) | 0.90 ± 0.22 |
| Mean reaction time, Stroop congruent trials (sec) | 1.31 ± 0.32 |
| Mean reaction time, MSIT congruent trials (sec) | 0.54 ± 0.11 |

### 3.2 Stressor-evoked cardiovascular reactivity

In the analytic sample, the resting baseline pre-stressor SBP and HR was 122 ± 11.6 mmHg and 67.4 ± 9.23 BPM, respectively (Table 1). Of the Stroop and MSIT readings, 3 SBP and 2 HR readings were deemed within-participants outliers (i.e., greater than 3 standard deviations from the respective participant mean) and were interpolated to the nearest neighbor. Consistent with prior reports on this sample (Gianaros et al., 2017; Sheu et al., 2012), the Stroop and MSIT together elicited significant increases in SBP (3.75 ± 5.11 mmHg, $t = 11.41$, $p < .001$) and HR (6.27 ± 4.87 BPM, $t = 20.01$, $p < .001$) across participants in the analytic sample (Figure 1). The mean within-participant correlation between SBP and HR was *rho* = .27 ± .02, $t = 13.71$, $p < .001$.

Two linear mixed models tested for task-related and condition-related differences in SBP and HR reactivity within participants, modeling task (Stroop, MSIT) and condition (incongruent, congruent) as fixed factors and participant as a random factor. There was a significant effect of condition for both SBP and HR, in which incongruent conditions elicited significantly greater reactivity than congruent conditions (SBP B ± SE = 1.23 ± 0.20, $t = 6.18$, $p < .001$; HR B ± SE = 2.11 ± 0.16, $t = 12.92$, $p < .001$). There was not a main effect of task on SBP nor HR (SBP B ± SE = 0.56 ± 0.44, $t = 1.26$, $p = .21$; HR B ± SE = 0.58 ± 0.36, $t = 1.58$, $p = .11$). However, there was a significant interaction of task and condition (SBP B ± SE = 0.57 ± 0.28, $t = 2.03$, $p = .04$; HR B ± SE = 0.80 ± 0.23, $t = 3.48$, $p < .001$) wherein there was greater reactivity during Stroop incongruent trials compared to other trials.

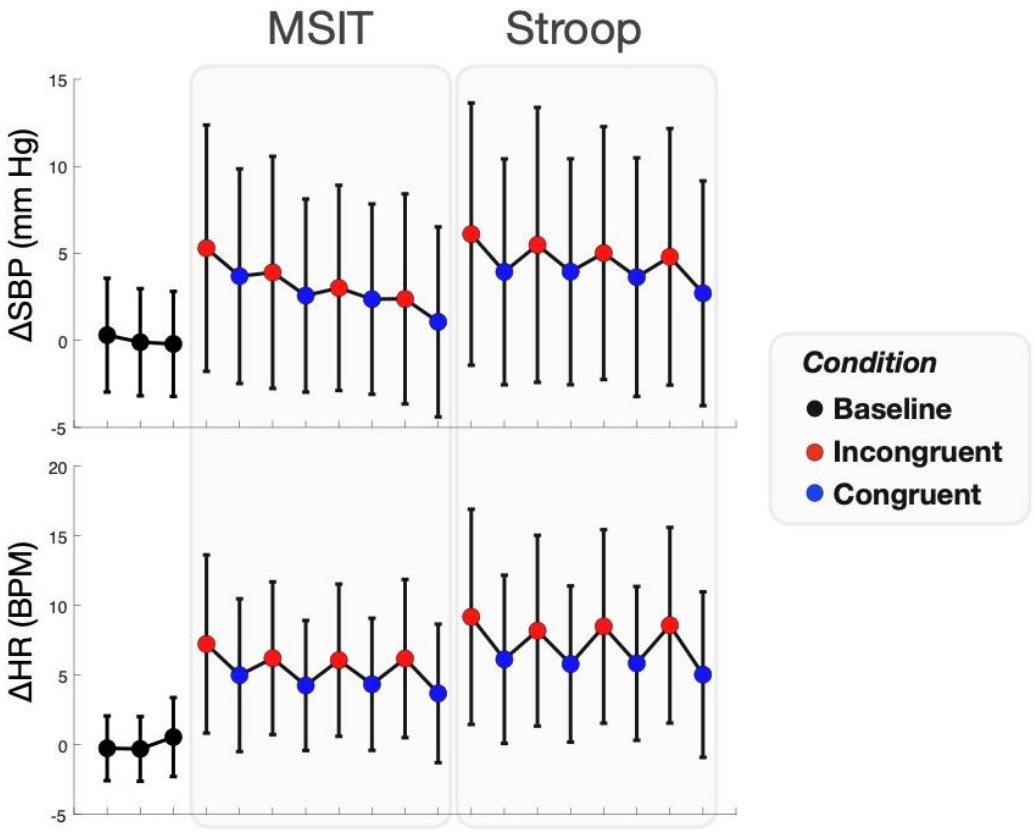


**Figure 1. Stressor-evoked cardiovascular reactivity.**

Panels depict the time course of change in systolic blood pressure (SBP; top) and heart rate (HR; bottom) reactivity during the baseline prestressor period, the MSIT, and the Stroop. Change scores were calculating by subtracting the mean of the participant's mean baseline readings. Circles reflect the group mean at each timepoint, and error bars reflect the group standard deviation (N = 242). Note that the order of administering the MSIT and Stroop was counterbalanced across participants but are grouped in this figure to illustrate task-related differences.

### 3.3 Stressor-evoked BOLD activity

Consistent with prior reports, the Stroop and MSIT engaged similar ensembles of brain regions commonly evoked by cognitive stressor paradigms (Akdeniz et al., 2014; Dedovic et al., 2005). Specifically, both tasks significantly activated the dorsolateral prefrontal cortex, dorsal anterior cingulate cortex, anterior insula, cerebellum, thalamus, periaqueductal gray, and pons (Figure 2; FDR < .05). Both tasks also significantly deactivated the ventromedial and orbitofrontal prefrontal cortex, amygdala, and hippocampus. The pattern of stressor-evoked BOLD activity was similar across the Stroop and MSIT (voxel-wise $r$ = .80; dice coefficient of thresholded maps = .79).

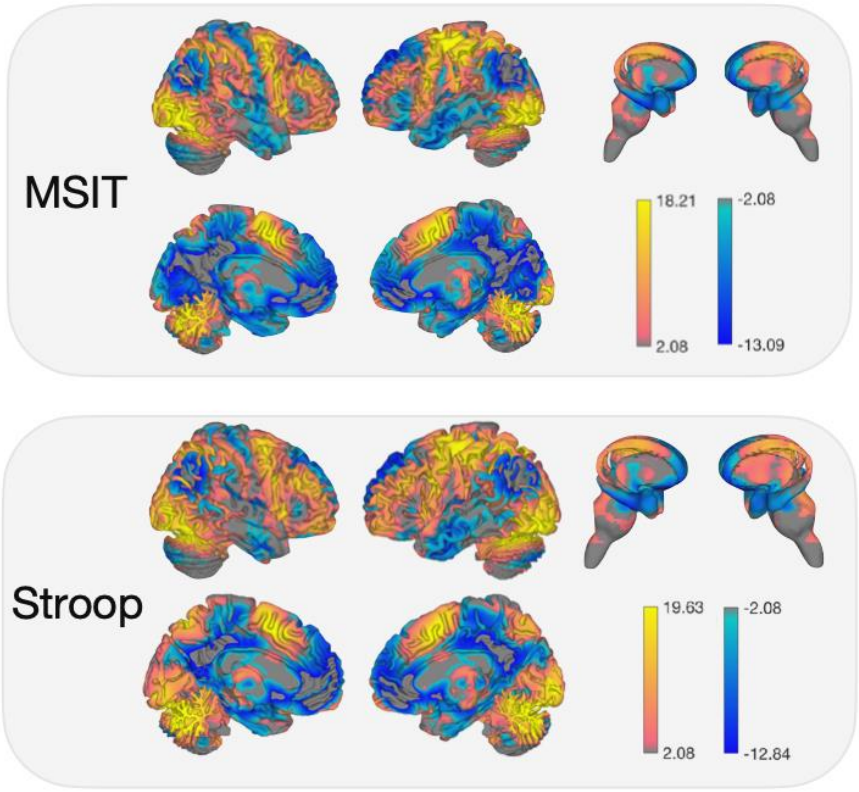


**Figure 2. Stressor-evoked BOLD activity.**

Color-scaled t-maps of brain areas exhibiting significant BOLD signal changes for the incongruent > congruent contrasts of the MSIT and Stroop. Maps are shown at a false discovery rate (FDR) threshold of 0.05 and extent threshold of 50 voxels. On the left, activation values are projected on the lateral and medial brain surfaces for both hemispheres. On the right, activation values are projected on limbic and brainstem volumes. Warmer colors (red/orange) reflect relative increases in activity, whereas cooler colors (blue) reflect relative decreases. Legends indicate the range of t-statistics depicted in each map.

### 3.4 Aim 1: Multivariate signatures of stressor-evoked cardiovascular reactivity

Primary analyses tested whether idiographic models implementing LASSO-PCR with cross-validation could reliably predict within-participant variation in SBP and HR. Figure 3 depicts distributions of predicted-observed Spearman's *rho* values for each model, and Table 2 presents summary statistics for Spearman's *rho* and other metrics of model performance. As described previously, idiographic whole-brain weight-maps were combined across participants to identify brain regions that consistently contributed to predictions. Considering that a portion of idiographic models described hereafter were found to not reliably predict within-participant in SBP and HR (see below), whole-brain voxel-wise weight-maps were nonetheless combined across all participants, thus including idiographic weight-maps of models that shrank all principal components to zero and therefore were uniformly comprised of zeros. These latter maps were included to conservatively adjust for the prevalence of so-called 'null' models.

#### 3.4.1 Hypothesis 1a: Idiographic prediction of SBP reactivity

The overall prediction of SBP within individuals was *rho* = -0.04 ± 0.04, $t$ = -0.94, $p$ = .345; $R^2$ = 0.05 ± 0.01; MAE = 3.14 ± 0.07; BF10 = 1.12 ± 0.10; BF01 = 2.51 ± 0.12 (Figure 3, left panel; Table 2, first row). That is, across participants, the overall distribution of within-participant Spearman's rank-order correlations between predicted and observed SBP was not significantly different from zero. These correlations ranged from -.99 to .85, with idiographic models predicting statistically significant variation (*rho* > 0 and $p$ < .05) in SBP reactivity in only 51 participants (21%) (Figure 3, left panel). Notably, in 46 participants (19%), the cross-validated LASSO shrank principal component features such that zero principal components were retained

in the final model; thus, for these participants, the model comprised a constant term and zero voxel weights. Moreover, the distribution of Bayes Factors suggested evidence in support of the null hypothesis. Hence, contrary to study hypotheses, a multivariate signature of brain activity did not reliably predict changes in SBP during psychological stress.

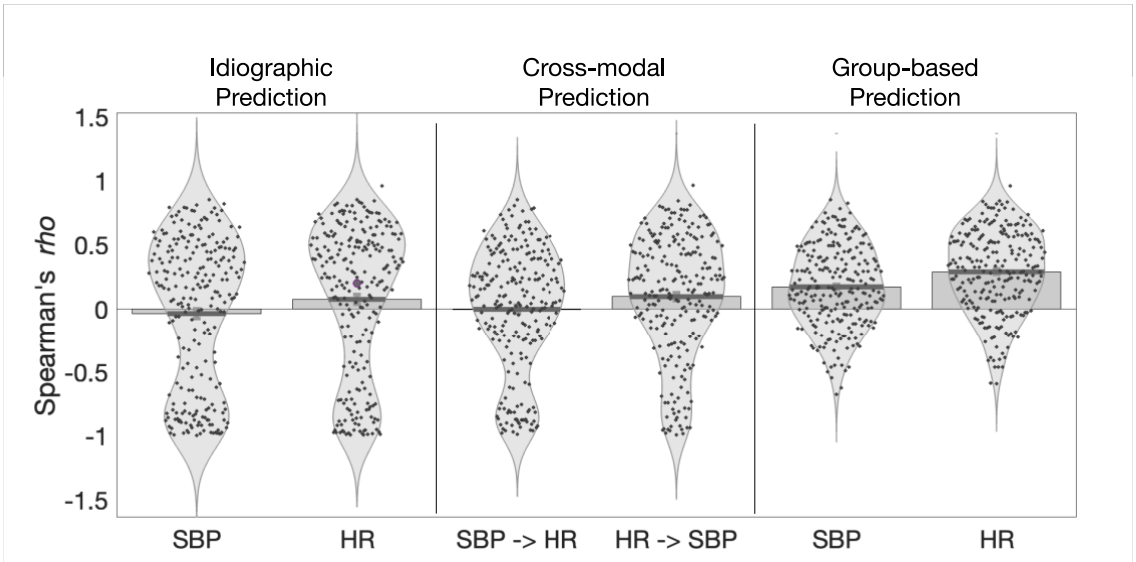


**Figure 3. Predictions of stressor-evoked cardiovascular reactivity using LASSO-PCR.**

Bar and violin plots depict distributions of predictions (i.e., predicted-observed Spearman's rho) for multivariate signature development using LASSO-PCR (Aim 1). Each point depicts the prediction of a participant. Lightly shaded bars depict the group mean, and dark shaded bars reflect the group standard error (N = 242). Violin plots depict the distribution shape. Left panel describes predictions for idiographic predictions trained to predict SBP and HR, respectively (Hypotheses 1a-1b). Middle panel describes predictions trained on one measure of physiology and tested on the other (Hypothesis 1c). Right panel describes predictions trained using group-based cross-validation (Hypothesis 1d).

**Table 2. Model performance of idiographic multivariate signatures using LASSO-PCR.**

Model performance across cardiovascular physiology (SBP, HR) and brain signatures for idiographic models using LASSO-PCR (Aim 1). Each model was evaluated according 4 sets of metrics describing the association between predicted and observed values: the Spearman's rank-order correlation (*rho*), coefficient of determination ($R^2$), mean absolute error (MAE), and Bayes Factors (BF10, BF01). Each statistic was reported using the group mean (M) and standard error (SE). In addition, the group distribution of Spearman's *rho* estimates was evaluated using a one-sample t-test.

| | ***rho*** | | | $R^2$ | **MAE** | **BF10** | **BF01** |
|---|---|---|---|---|---|---|---|
| | M ± SE | *t* | *p* | M ± SE | M ± SE | M ± SE | M ± SE |
| *Idiographic prediction* | | | | | | | |
| SBP | -.04 ± .04 | -0.94 | .345 | 0.05 ± 0.01 | 3.14 ± 0.07 | 1.12 ± 0.10 | 2.51 ± 0.12 |
| HR | .08 ± .04 | 2.00 | .047 | 0.11 ± 0.02 | 2.44 ± 0.08 | 1.33 ± 0.10 | 2.25 ± 0.12 |
| *Cross-modal prediction* | | | | | | | |
| SBP -> HR | .00 ± .03 | -0.06 | .947 | -0.99 ± 0.06 | 5.35 ± 0.22 | 0.36 ± 0.02 | 3.64 ± 0.09 |
| HR -> SBP | .10 ± .03 | 3.12 | .002 | -0.81 ± 0.28 | 5.55 ± 0.21 | 0.46 ± .03 | 3.43 ± 0.11 |
| *Group-based prediction* | | | | | | | |
| SBP | .17 ±.02 | 8.48 | < .001 | -0.63 ± 0.04 | 5.68 ± 0.22 | 0.33 ± 0.01 | 2.95 ± 0.12 |
| HR | .29 ± .02 | 13.92 | < .001 | -0.41 ± 0.04 | 6.53 ± 0.27 | 0.37 ± 0.02 | 2.43 ± 0.12 |

A one-sample t-test of the within-participant signatures of SBP reactivity revealed several brain areas that consistently contributed to idiographic SBP models (FDR < .05, k > 50 voxel threshold). Specifically, and consistent with study hypotheses, SBP was predicted by positive weights in the dorsal anterior cingulate cortex. In addition, SBP was predicted by positive weights in the dorsolateral prefrontal cortex, and cerebellum, and by negative weights in the caudate and putamen (Figure 4; Table 3). The strength of voxel weights in the thresholded signature was moderately correlated with voxel weights in the average main effects map reported above ($r$ = .36). However, brain regions observed in the thresholded signature predicting SBP did not strongly

overlap with those observed in the thresholded Stroop and MSIT main effects maps (dice coefficients < .04).

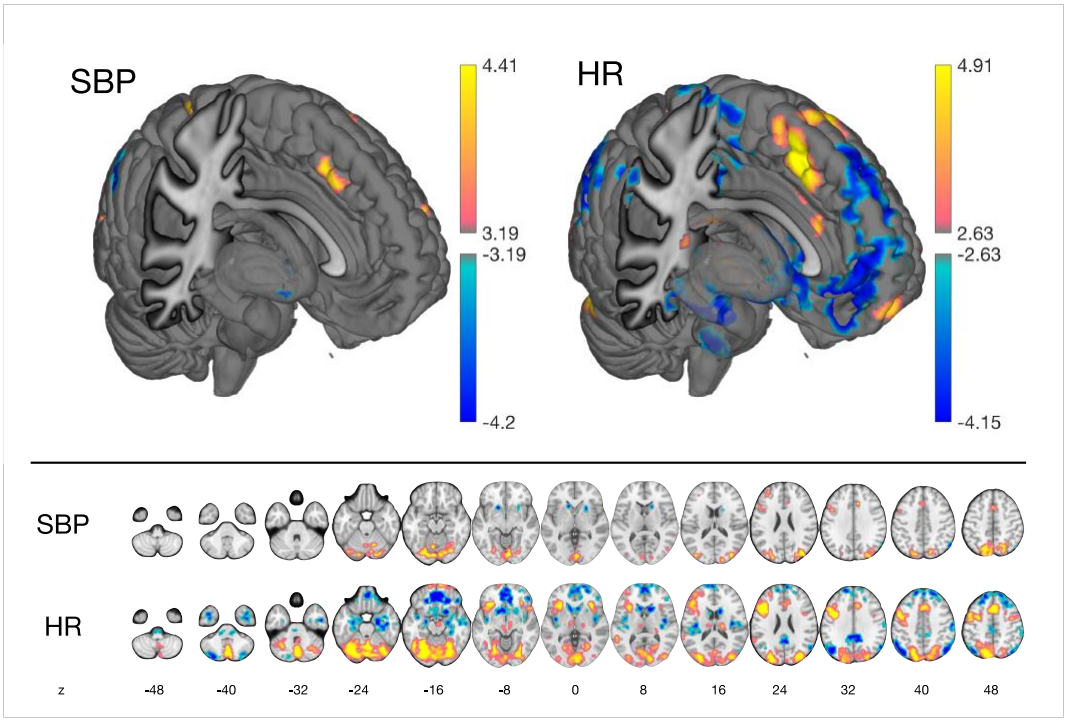


**Figure 4. Brain regions consistently contributing to idiographic models of SBP and HR.**

Regions were identified by conducting a voxel-wise one-sample t-test on idiographic predictive maps and applying a false discovery rate (FDR) threshold of 0.05 and extent threshold of 50 voxels. Top panel depicts significant clusters identified in SBP (left) and HR (right) models and are projected onto a cutaway surface. Bottom panel depicts a series of axial slices on the whole-brain volume. Warm colors (red/orange) reflect positive weights, and cool colors (blue) reflect negative weights.

**Table 3. Brain regions consistently contributing to idiographic models of SBP.**

Regions were identified by conducting a voxel-wise one-sample t-test on idiographic predictive maps and applying a false discovery rate (FDR) threshold of 0.05 and extent threshold of 50 voxels.

| Effect Direction | Region Label | Peak MNI Coordinates | | | Voxels | Peak Weight |
|---|---|---|---|---|---|---|
| | | X | Y | Z | | |
| Positive | Dorsal Anterior Cingulate Cortex | 0 | 18 | 44 | 356 | 4.57 |
| | Dorsal Anterior Cingulate Cortex | 8 | 24 | 30 | 134 | 4.55 |
| | Dorsolateral Prefrontal Cortex | -32 | 4 | 58 | 174 | 4.47 |
| | Dorsolateral Prefrontal Cortex | -32 | 44 | 22 | 260 | 4.39 |
| | Dorsolateral Prefrontal Cortex | -46 | 12 | 30 | 432 | 4.92 |
| | Superior Parietal Gyrus | 10 | -70 | 44 | 4151 | 6.00 |
| | Visual Cortex | -30 | -82 | 20 | 557 | 4.59 |
| | Cerebellum | 0 | -80 | -12 | 3588 | 5.50 |
| | Cerebellum | -6 | -64 | -18 | 253 | 4.72 |
| | Cerebellum | 12 | -62 | -22 | 140 | 4.70 |
| Negative | Occipital Lobe | 54 | -60 | 38 | 195 | -4.58 |
| | Visual Cortex | 14 | -90 | 14 | 222 | 4.24 |
| | Caudate, Putamen | 18 | 14 | 4 | 287 | -4.46 |
| | Caudate, Putamen | -14 | 16 | -4 | 217 | -5.10 |

### 3.4.2 Hypothesis 1b: Idiographic prediction of HR reactivity

The overall prediction of HR within individuals was *rho* = 0.08 ± 0.04, $t = 2.00$, $p = .047$; $R^2 = 0.11 \pm 0.02$; MAE = 2.44 ± 0.08; BF10 = 1.33 ± 0.10; BF01 = 2.25 ± 0.12. That is, although the distribution of within-participant Spearman's rank-order correlations between predicted and observed HR were significantly different from zero according to standard conventions, there was substantial variation in performance of the idiographic models. These correlations ranged from -.99 to .96, with idiographic models predicting statistically significant variation (*rho* > 0 and $p < .05$) in HR reactivity in only 74 participants (30%) (Figure 3, left panel). Notably, in 40 participants (16.5%), the cross-validated LASSO shrank all principal component features such that zero

principal components were retained in the final model; thus, for these participants, the model comprised a constant term and zero voxel weights. Moreover, the distribution of Bayes Factors suggested evidence in support of the null hypothesis. Hence, contrary to study hypotheses, a multivariate signature of brain activity did not reliably predict changes in HR during psychological stress, even though the distribution of Spearman's *rho'*s were statistically different from zero.

A one-sample t-test of the within-participant signatures of HR reactivity revealed several brain areas that consistently contributed to idiographic HR models (FDR < .05, k > 50 voxel threshold). Consistent with study hypotheses, HR was predicted by positive weights in the anterior insula, and by negative weights in the medial prefrontal cortex and amygdala. In addition, HR was predicted by positive weights in the dorsal anterior cingulate cortex, dorsolateral prefrontal cortex, inferior parietal lobule, cerebellum, and midbrain, and by negative weights in the posterior insula, hippocampus, caudate, and putamen (Figure 4; Table 4). The strength of voxel weights in the unthresholded signature was moderately correlated with voxel weights in the average main effects map reported above ($r$ = .56). Moreover, brain regions observed in the thresholded signature predicting HR overlapped moderately with regions observed in the thresholded Stroop and MSIT main effects maps (dice coefficients > .20).

Comparing the predictive performance of the above idiographic models revealed that idiographic HR models were significantly more predictive than idiographic SBP models, as evidenced by significantly higher predicted-observed Spearman's *rho* values (paired $t$ = 3.08, $p$ = .002), higher $R^2$ values (paired $t$ = 2.32, $p$ = .021), and lower MAE values (paired $t$ = -7.88, $p$ < .001). By contrast, the idiographic SBP and HR models did not significantly differ in terms of Bayes Factors.

**Table 4. Brain regions consistently contributing to idiographic models of HR.**

Regions were identified by conducting a voxel-wise one-sample t-test on idiographic predictive maps and applying a false discovery rate (FDR) threshold of 0.05 and extent threshold of 50 voxels.

| Effect Direction | Region Label | Peak MNI Coordinates | | | Voxels | Peak Weight |
|---|---|---|---|---|---|---|
| | | X | Y | Z | | |
| Positive | Premotor Cortex, Dorsolateral Prefrontal Cortex | -24 | 10 | 42 | 10245 | 7.03 |
| | Dorsolateral Prefrontal Cortex | 42 | 6 | 28 | 183 | 4.02 |
| | Medial Prefrontal Cortex | 10 | 62 | -14 | 880 | 5.22 |
| | Superior Parietal Gyrus | -62 | -44 | 22 | 209 | 3.99 |
| | Superior Temporal Gyrus | -56 | -44 | 8 | 213 | 4.47 |
| | Anterior Insula | 36 | 22 | 0 | 718 | 5.69 |
| | Cerebellum, Visual Cortex | -4 | -74 | 4 | 23577 | 6.84 |
| | Thalamus | 16 | -20 | 14 | 290 | 4.77 |
| | Thalamus | -10 | -16 | 8 | 376 | 4.16 |
| | Substantia Nigra | 4 | -18 | -8 | 646 | 3.95 |
| Negative | Medial Prefrontal Cortex | 6 | 48 | 6 | 8780 | -5.98 |
| | Superior Parietal Gyrus | 58 | -22 | 40 | 654 | -4.65 |
| | Superior Parietal Gyrus | 48 | -64 | 38 | 1160 | -5.08 |
| | Inferior Temporal Gyrus | -38 | 4 | -38 | 258 | -4.17 |
| | Superior Parietal Gyrus | -46 | -66 | 38 | 1535 | -5.80 |
| | Somatomotor Cortex | -36 | -26 | 62 | 255 | -4.30 |
| | Somatomotor Cortex | 4 | -28 | 72 | 688 | -4.45 |
| | Posterior Cingulate | -4 | -26 | 48 | 273 | -3.72 |
| | Posterior Cingulate | 2 | -44 | 30 | 1362 | -4.64 |
| | Amygdala | 32 | -10 | -24 | 2464 | -5.26 |
| | Amygdala | -24 | -12 | -20 | 844 | -4.73 |
| | Posterior Insula | -40 | -4 | 0 | 384 | -4.78 |
| | Posterior Insula | 40 | -10 | 10 | 827 | -4.79 |
| | Posterior Insula | -42 | -22 | 14 | 733 | -4.29 |
| | Caudate, Putamen | -4 | 14 | 0 | 1919 | -5.30 |
| | Putamen | 18 | 12 | -10 | 459 | -4.97 |
| | Cerebellum | 28 | -80 | -36 | 289 | -4.04 |
| | Cerebellum | -28 | -80 | -36 | 564 | -4.83 |
| | Brainstem | 4 | -32 | -42 | 286 | -4.08 |
| | Brainstem | -8 | -28 | -34 | 191 | -3.74 |

The unthresholded weight-maps reflecting the overall idiographic predictions of SBP and HR were positively correlated across voxels ($r$ = .65). By contrast, the thresholded weight-maps (FDR < .05, k > 50 voxel threshold) showed only modest overlap in terms of their suprathreshold regions (dice coefficien*t* = .13). Comparing the overall weight-maps using paired t-tests revealed there were no significant differences in the weight maps in terms of individual voxel weights when thresholded at FDR < .05, k > 50 voxels.

### 3.4.3 Hypothesis 1c: Cross-modal prediction

The idiographic models trained on SBP and HR reactivity were tested on the other metric of cardiovascular physiology for each participant. The idiographic LASSO-PCR models trained to predict SBP and tested on HR showed unreliable prediction of HR, overall *rho* = .00 ± .03, $t$ = -0.06, $p$ = .947; $R^2$ = -0.99 ± 0.06; MAE = 5.35 ± 0.22; BF10 = 0.36 ± 0.02; BF01 = 3.64 ± 0.09 (Table 2 and Figure 3, middle panel). Although this result was contrary to study hypotheses, it was somewhat expected in the context of the failure to develop reliable idiographic models of SBP (Hypothesis 1a, above). Finally, the strength of this prediction (*rho*) did not significantly differ from the idiographic prediction of SBP described previously (paired $t$ = 1.72, $p$ = .09).

The idiographic LASSO-PCR models trained to predict HR and tested on SBP showed somewhat reliable prediction of SBP, *rho* = .10 ± .03, $t$ = 3.12, p =.002; $R^2$ = -0.81 ± 0.28; MAE = 5.55 ± 0.21; BF10 = 0.46 ± .03; BF01 = 3.43 ± 0.11. However, the strength of this prediction did not significantly differ from the idiographic prediction of HR (paired $t$ = 0.91, $p$ = .365), which was contrary to study hypotheses as well as the findings of Eisenbarth et al. (2016).

### 3.4.4 Hypothesis 1d: Group-based prediction

In addition to testing the generalizability of idiographic models across measures of cardiovascular physiology, models were also tested in terms of their generalizability to new individuals. Thus, 10-fold cross-validated predictions stratifying across mean levels of stressor-evoked cardiovascular reactivity showed modestly reliable prediction of SBP, overall *rho* = .17 ±.02, $t$ = 8.48, $p < .001$; $R^2$ = -0.63 ± 0.04; MAE = 5.68 ± 0.22; BF10 = 0.33 ± 0.01; BF01 = 2.95 ± 0.12 (Table 2, bottom panel; Figure 4, right panel). Contrary to study hypotheses, the group-based prediction of SBP was significantly more predictive than the idiographic prediction of SBP (paired $t$ = 5.69 $p < .001$) and HR (paired $t$ = 2.66 $p$ = .008).

Similarly, the group-based prediction of HR was also modestly reliable, overall *rho* = .29 ± .02, $t$ = 13.92; $p < .001$; $R^2$ = -0.41 ± 0.04; MAE = 6.53 ± 0.27; BF10 = 0.37 ± 0.02; BF01 = 2.43 ± 0.12. Contrary to study hypotheses, the group-based prediction of HR was significantly more predictive than the idiographic prediction of SBP (paired $t$ = 8.02, $p < .001$) and HR (paired $t$ = 6.02, $p < .001$), and it was also significantly more predictive than the group-based prediction of SBP (paired $t$ = 5.11, $p < .001$).

## 3.5 Aim 2: Generalizability of published multivariate signatures

### 3.5.1 Hypothesis 2a: Commonalities between published and empirical brain signatures.

The prediction weights of the published signatures by Eisenbarth et al. (2016) and Gianaros et al. (2017) were not strongly correlated across voxels, $r$ = .04 (Figure 5). Notably, and consistent

with study hypotheses, prediction weights in the signature by Eisenbarth et al. were modestly correlated with the prediction weights in the idiographic SBP ($r$ = .16) and idiographic HR ($r$ = .20) signatures developed in Aim 1. By contrast, prediction weights in the signature by Gianaros et al. were not strongly correlated with the prediction weights in either idiographic signature developed in Aim 1 (r's < .06).

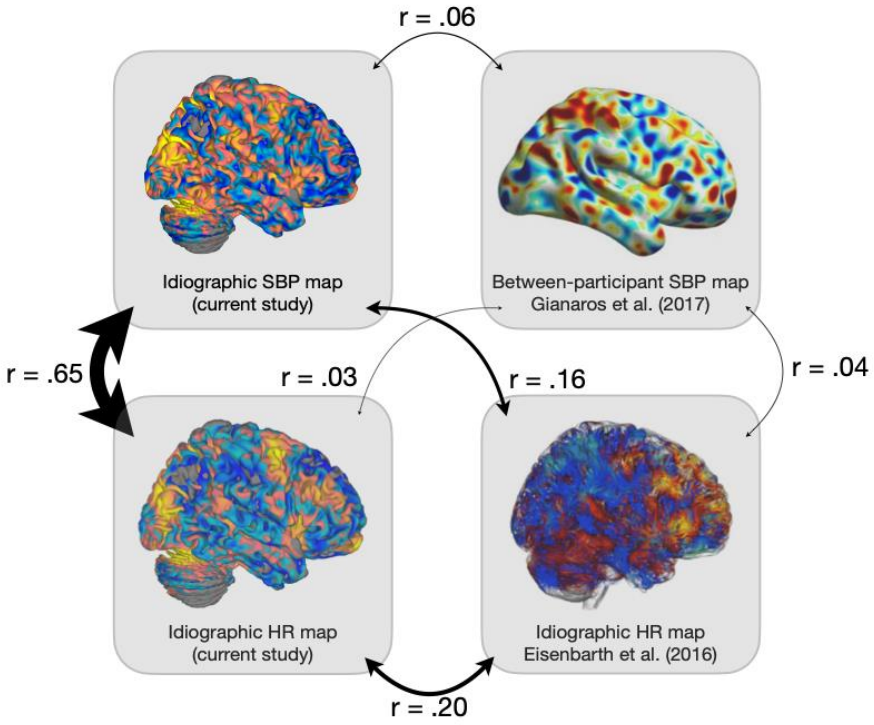


**Figure 5. Commonalities between published and empirical brain signatures.**

Each panel depicts a lateral hemisphere surface rendering of empirical (top left; bottom left) and previously published (top right; bottom right) multivariate brain signatures of stressor-evoked cardiovascular reactivity. Connections between each signature reports the voxel-wise association (Pearson $r$) between each pattern. The thickness of each arrow corresponds to the effect size of the association.

### 3.5.2 Hypothesis 2b: Generalizability of Gianaros et al. (2017)

Applying the unthresholded published signatures to the block-specific beta maps in the analytic sample to predict SBP and HR revealed appreciable variability in predictive performance (Figure 6; Table 5). Specifically, applying the published signature by Gianaros et al. to predict within-participant changes in SBP revealed an overall *rho* = .05 ± .02, range -.67 to .75, $t$ = 2.79, $p$ = .005; $R^2$= -0.85 ± 0.04; MAE = 5.80 ± 0.22; BF10 = 0.29 ± 0.01; BF01 = 3.91 ± 0.07. Finally, applying the published signature by Gianaros et al. to predict within-participant changes in HR revealed an overall *rho* = .09 ± .02, range -.67 to .85, $t$ = 4.82, $p$ < .001; $R^2$ = -0.80 ± 0.04; MAE = 6.82 ± 0.28; BF10 = 0.27 ± .01; BF01 = 4.07 ± 0.07. The signature of Gianaros et al. did not significantly differ in terms of its prediction of SBP and HR ($t$ = 1.56, $p$ = .121). Thus, contrary to study hypotheses, the multivariate signature of individual differences in SBP reactivity as reported by Gianaros et al. was found to modestly predict within-participant changes in SBP and HR in this sample. However, it should be noted that the observed effect size of this prediction was smaller than the effect originally reported by Gianaros et al. (hold-out test sample $r$ = .32).

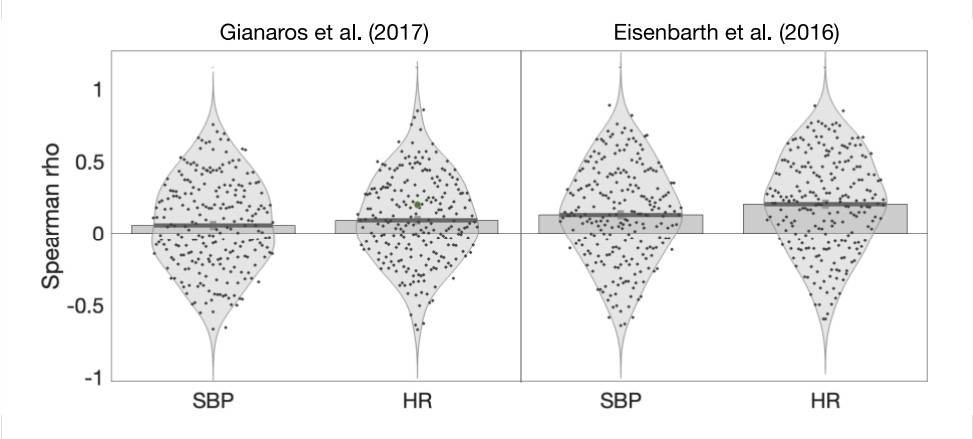


**Figure 6. Generalizability of previously published brain signatures.**

Bar and violin plots depict distributions of predictions (i.e., predicted-observed Spearman's *rho*) of SBP and HR reactivity from published brain signatures (Aim 2). Each point depicts the prediction of a participant. Lightly shaded bars depict the group mean, and dark shaded bars reflect the group standard error (N = 242). Violin plots depict the distribution shape. Left panel depicts idiographic predictions from the signature of individual differences in SBP reactivity by Gianaros et al. (2017) (Hypothesis 2b). Right panel depicts idiographic predictions from the signature of HR reactivity by Eisenbarth et al. (2016) (Hypothesis 2c).

**Table 5. Generalizability of previously published brain signatures.**

Each model was evaluated according 4 sets of metrics describing the association between predicted and observed values: the Spearman's rank-order correlation (*rho*), coefficient of determination ($R^2$), mean absolute error (MAE), and Bayes Factors (BF10, BF01). Each statistic was reported using the group mean (M) and standard error (SE). In addition, the group distribution of Spearman's *rho* estimates was evaluated using a one-sample t-test.

| | ***rho*** | | | ***$R^2$*** | **MAE** | **BF10** | **BF01** |
|---|---|---|---|---|---|---|---|
| | M ± SE | *t* | *p* | M ± SE | M ± SE | M ± SE | M ± SE |
| *Gianaros et al. (2017)* | | | | | | | |
| SBP | .05 ± .02 | 2.79 | .005 | -0.85 ± 0.04 | 5.80 ± 0.22 | 0.29 ± 0.01 | 3.91 ± 0.07 |
| HR | .09 ± .02 | 4.82 | < .001 | -0.80 ± 0.04 | 6.82 ± 0.28 | 0.27 ± .01 | 4.07 ± 0.07 |
| *Eisenbarth et al. (2016)* | | | | | | | |
| SBP | .13 ± .02 | 6.09 | < .001 | -0.74 ± 0.04 | 5.79 ± 0.22 | 0.30 ± 0.01 | 3.83 ± 0.08 |
| HR | .20 ± .02 | 9.67 | < .001 | -0.58 ± 0.04 | 6.81 ± 0.28 | 0.37 ± 0.01 | 3.45 ± 0.09 |

### 3.5.3 Hypothesis 2c: Generalizability of Eisenbarth et al. (2016)

Applying the published signature by Eisenbarth et al. to predict within-participant changes in HR revealed an overall *rho* = .20 ± .02, range -.60 to .88, $t$ = 9.67, $p$ < .001; $R^2$= -0.58 ± 0.04; MAE = 6.81 ± 0.28; BF10 = 0.37 ± 0.01; BF01 = 3.45 ± 0.09. In addition, applying this published signature to predict within-participant changes in SBP revealed an overall *rho* = .13 ± .02, range -.64 to .89, $t$ = 6.09, $p$ < .001; $R^2$= -0.74 ± 0.04; MAE = 5.79 ± 0.22; BF10 = 0.30 ± 0.01; BF01 = 3.83 ± 0.08. The signature of Eisenbarth et al. was significantly more predictive of HR than of SBP ($t$ = 3.25, $p$ = .001). Thus, contrary to study hypotheses, the multivariate signature of within-participant changes in HR reactivity as reported by Eisenbarth et al. was found to modestly predict within-participant changes in HR and SBP in this sample. However, it should be noted that the observed effect size of this prediction was smaller than the effect originally reported by Eisenbarth et al. (cross-validated $r$ = .54).

## 3.6 Planned supplementary analyses

### 3.6.1 Local spatial similarity analyses and network analyses of signatures

In addition to comparing the multivariate signatures from Aim 1 on a voxel-wise basis, planned supplementary analyses additionally compared these signatures based on local patterns of prediction weights, as well as their correspondence with large-scale intrinsic networks. First, local searchlight analyses were conducted on each participant for whom the idiographic LASSO-PCR routine generated voxel-wise predictive weight-maps for both SBP and HR (N = 165). Combining

the resulting searchlight maps across participants and applying an FDR threshold of .05 and extent threshold of 50 voxels revealed that nearly the entire volume (96.8% of gray matter voxels) showed a significant positive covariation in the local pattern between idiographic SBP and HR maps. This result was likely due to a combination of the strong association between the two sets of weight-maps (group-level voxel-wise r = .65) plus the large sample size for conducting one-sample t-tests. By contrast, no regions exhibited significant negative local covariation in the local patterns between maps. Considering this result, the resulting searchlight map was thresholded to show the top 5$^{th}$ percentile of voxels showing the strongest local pattern similarity across voxels (Figure 7; mean $r$ > .28; $t$ > 7.88). This map revealed strongest estimates of local pattern similarity in the anterior cingulate cortex, medial prefrontal cortex, dorsolateral prefrontal cortex, anterior insula, and visual cortex (Figure 7).

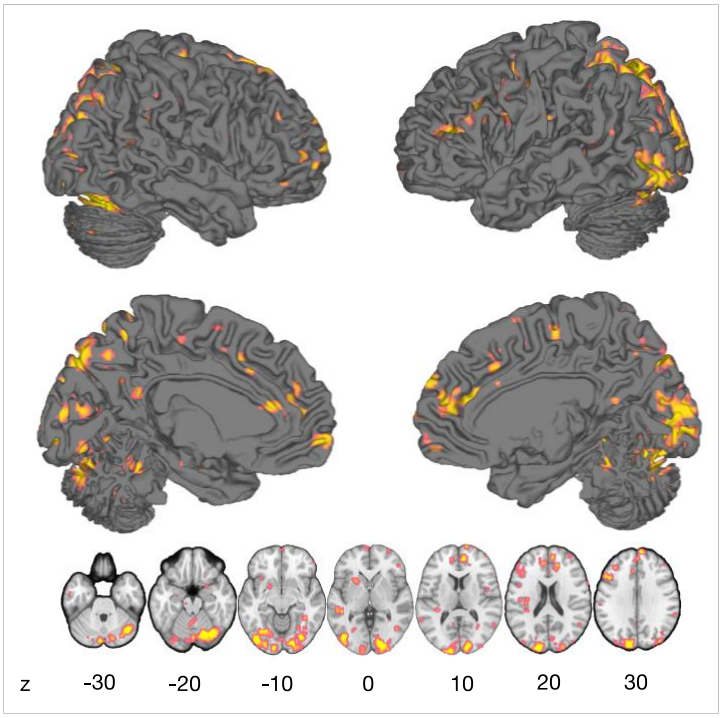


**Figure 7. Local spatial similarity analyses.**

Similarity maps were thresholded to depict voxels showing greater than 95$^{th}$ percentile in the average local spatial correlation at neighboring voxels.

The similarity of individual multivariate signatures was assessed with large-scale intrinsic brain networks, and these similarity metrics were combined across participants (Figure 8; Table 6). The SBP signature showed significant positive correspondence with the dorsal attention ($t$ = 4.31, $p$ < .001), ventral attention ($t$ = 2.78, $p$ =.006), frontoparietal ($t$ = 2.39, $p$ = .018), and visual ($t$ = 4.89, $p$ < .001) networks. The HR signature showed significant correspondence with all but one network: specifically, it showed positive correspondence with the dorsal attention ($t$ = 3.07, $p$ < .001), frontoparietal ($t$ = 3.31, $p$ = .001), and visual ($t$ = 7.50, $p$ <.001) networks, as well as negative correspondence with the somatomotor ($t$ = -2.17, $p$ = .031), limbic ($t$ = -3.04, $p$ = .003), and default mode ($t$ = -2.81, $p$ = .005) networks. There were significant differences between the SBP and HR signatures in terms of their correspondence with these networks: the SBP signature showed significantly greater correspondence with the somatomotor (paired $t$ = 2.30, $p$ = .022) and limbic network (paired $t$ = 2.78, $p$ = .005), whereas the HR signature showed significantly greater correspondence with the visual network ($t$ = 2.05, $p$ = .041).

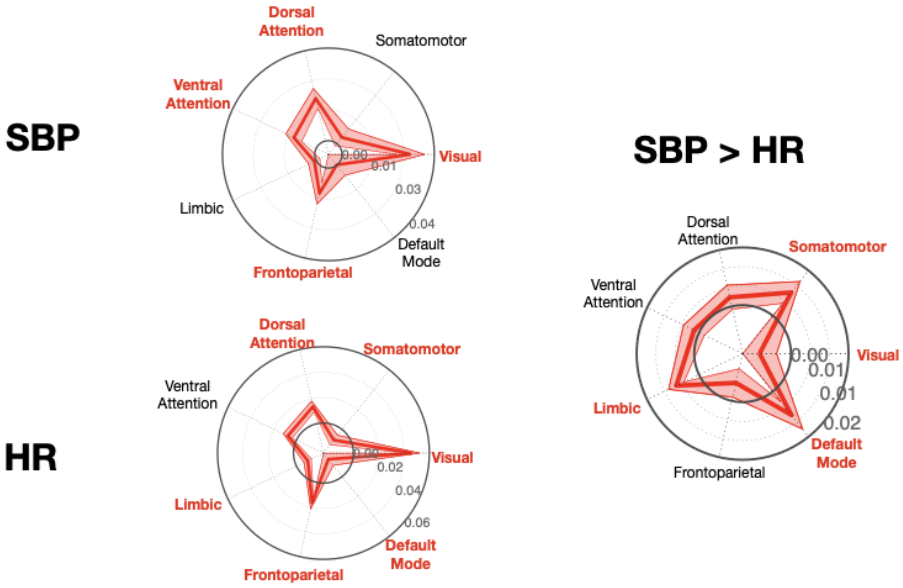


**Figure 8. Network similarity analyses of SBP and HR signatures.**

Polar plots depict the mean ± SE of correspondence between each multivariate signature and large-scale intrinsic networks. Right panel: paired t-test of the correspondence between SBP and HR signatures and intrinsic networks. Networks with a significant effect ($p < .05$) are labeled in red.

**Table 6. Correspondence between multivariate signatures and large-scale intrinsic brain networks.**

| | SBP | | | HR | | | Difference (SBP > HR) | |
|---|---|---|---|---|---|---|---|---|
| | **mean *r*** | ***t*** | ***p*** | **mean *r*** | ***t*** | ***p*** | **paired *t*** | ***p*** |
| Somatomotor | .00 | 0.74 | .461 | -.01 | -2.17 | .031 | 2.30 | .022 |
| Dorsal Attention | .02 | 4.31 | < .001 | .01 | 3.07 | .002 | 0.96 | .337 |
| Ventral Attention | .01 | 2.78 | .006 | .01 | 1.87 | .062 | 0.71 | .476 |
| Limbic | .00 | 0.32 | .752 | -.01 | -3.04 | .003 | 2.78 | .005 |
| Frontoparietal | .01 | 2.39 | .018 | .02 | 3.31 | .001 | -0.74 | .456 |
| Default Mode | .00 | -0.02 | .982 | -.02 | -2.81 | .005 | 2.22 | .027 |
| Visual | .03 | 4.89 | < .001 | .05 | 7.50 | < .001 | -2.05 | .041 |

### 3.6.2 Psychometric properties of brain signatures

The median Spearman-Brown internal consistency of Stroop and MSIT voxels were 0.46 and 0.41, respectively, whereas the maximum internal consistency for the Stroop and MSIT voxels were 0.89 and 0.87, respectively. The Stroop demonstrated significantly greater internal consistency across voxels than the MSIT, paired $t = 223.46$, $p < .001$. The Stroop and MSIT internal consistency maps were correlated across voxels, $r = .75$; thus, the Stroop and MSIT internal consistency maps were combined into a map depicting the average internal consistency at each voxel.

Figure 9 depicts the whole-brain maps comprising voxel-wise estimates of internal consistency for the Stroop and MSIT, as well as their average. These maps were thresholded to depict ranges of consistency considered to be 'fair' ($r_{SB}$ range .4 to .6, red), 'good' ($r_{SB}$ range .6 to .75, yellow), and 'excellent' ($r_{SB} > .75$, green). In the Stroop, 34,650 voxels (16.7%) exhibited 'good' and an additional 7,474 voxels (3.6%) exhibited 'excellent' consistency, whereas in the MSIT, 25,808 voxels (12.4%) exhibited 'good' and an additional 2,417 voxels (1.6%) exhibited 'excellent' consistency. Regions exhibiting 'good-to-excellent' consistency ($r_{SB} > 0.6$) when averaged across the Stroop and MSIT and surviving an extent threshold of 50 voxels included regions such as the ventromedial prefrontal cortex, dorsolateral prefrontal cortex, primary motor cortex, and somatosensory cortex (Table 7).

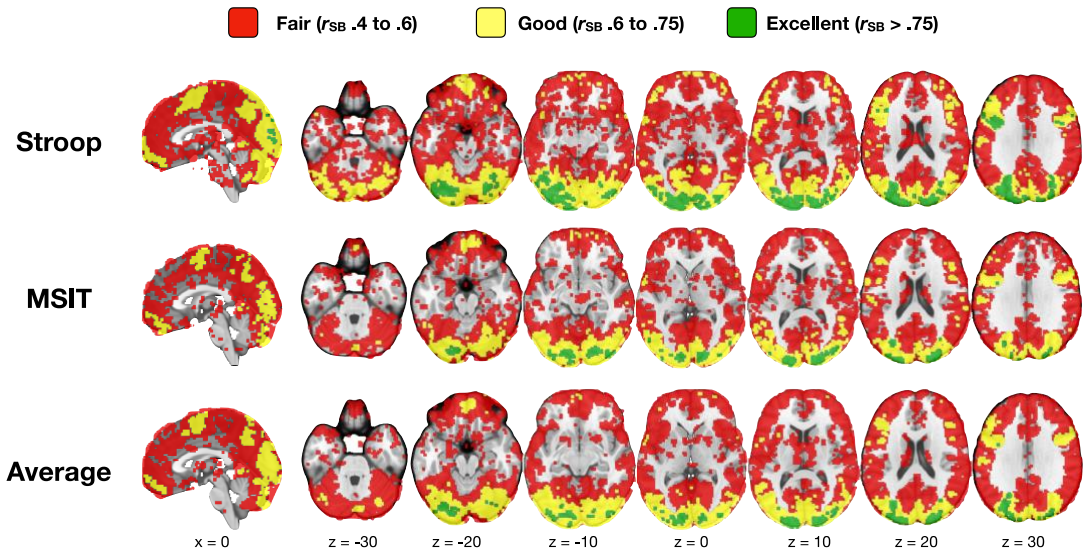


**Figure 9. Internal consistency of the Stroop, MSIT, and their average.**

Whole-brain voxel-wise maps that depict the split-half internal consistency of the Stroop and MSIT, as well as a map depicting the average internal consistency of both tasks. Voxels are shaded according to whether they fall in the 'fair' ($r_{SB}$ range .4 to .6), 'good' ($r_{SB}$ range .6 to .75) or 'excellent' ($r_{SB}$ > .75) range. Clusters showing 'good to excellent' internal consistency in the average internal consistency map are described in Table 7.

**Table 7. Regions demonstrating good-to-excellent internal consistency.**

These regions (Spearman-Brown corrected $r$ > .6) are depicted in green color in Figure 9.

| Region Label | Peak MNI Coordinates | | | Voxels | Peak $r_{SB}$ |
|---|---|---|---|---|---|
| | X | Y | Z | | |
| Ventromedial Prefrontal Cortex | 0 | 54 | -16 | 570 | 0.70 |
| Dorsolateral Prefrontal Cortex | 44 | 26 | 18 | 150 | 0.67 |
| Lateral Prefrontal Cortex; Occipital Cortex | -18 | -70 | 28 | 44104 | 0.85 |
| Primary Motor Cortex | 42 | 4 | 48 | 2781 | 0.78 |
| Somatosensory Cortex | -2 | 4 | 56 | 977 | 0.72 |

Associations between internal consistency, main effects of BOLD activity (incongruent > congruent contrast), and prediction beta weights were explored across voxels (Figure 10). These scatterplots suggested that internal consistency tended to constrain the magnitude of the main effect contrast parameter for a given voxel (Panel A). In other words, the maximum absolute main effect that a voxel could elicit was in part limited according to its internal consistency. In addition, these scatterplots showed that main effects tended to correlate positively with multivariate signature prediction weights (Panel B & C). Finally, these scatterplots similarly showed that internal consistency tended to constrain the magnitude of multivariate signature prediction weights (Panel D & C).

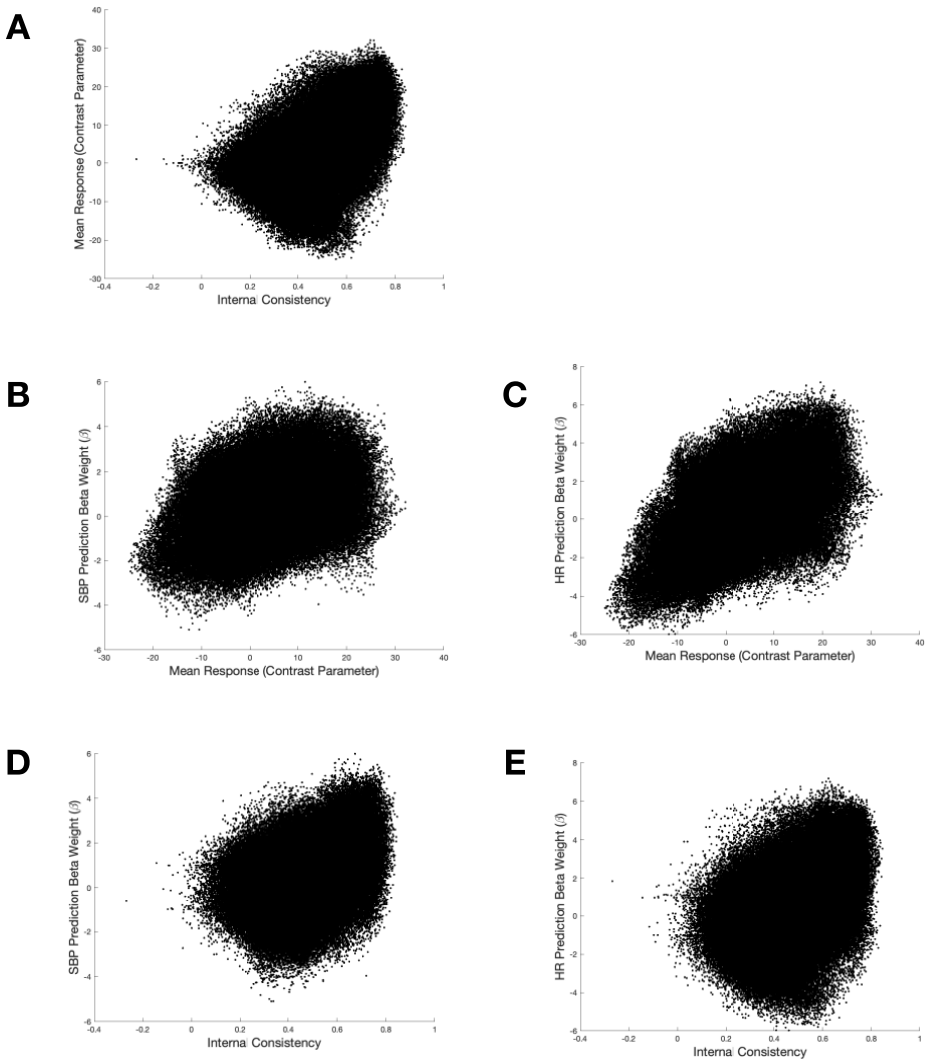


**Figure 10. Comparisons of mean response, internal consistency, and prediction weights.**

Scatterplots depict voxel-wise associations between mean reasonse, internal consistency (Spearman-Brown corrected *r*), and prediction weights. Mean response refers to the incongruent > congruent contrast averaged across the Stroop and MSIT.

### 3.6.3 Contribution of nuisance variables

To examine whether physiological or motion-related artifacts may play a potentially confounding role in predicting stressor-evoked SBP or HR reactivity, two sets of sensitivity

analyses repeated the idiographic LASSO-PCR approach used in Aim 1, this time replacing whole-brain BOLD beta maps with block-related averages in white matter and cerebrospinal fluid signals, as well as block related averages in head motion estimates.

The first sensitivity analysis used the mean white matter and cerebrospinal fluid signals plus their temporal derivatives and squares (see section 2.3.3). These analyses revealed uniformly poor performance in the ability to reliably predict SBP and HR (Table 8, top panel). Predictions of SBP and HR by these physiological signals were significantly worse than the idiographic models using whole-brain BOLD beta maps in Aim 1 ($t$'s < -5.42, $p$'s < .001).

Similarly, the second set of sensitivity analyses repeated the first, adding head motion estimates to the white matter and cerebrospinal fluid signal, and incorporating temporal derivatives and squares (see section 2.3.3). These models also revealed uniformly poor performance in the ability to reliably predict SBP and HR reactivity (Table 8, bottom panel). Whereas the prediction of SBP by these physiological signals and head motion estimates was not significantly worse than the idiographic models using whole-brain BOLD beta maps in Aim 1 ($t$ = -1.28, $p$ = .20), the prediction of HR was indeed significantly worse than the idiographic model derived in Aim 1 ($t$ = -2.32, $p$ = .02).

**Table 8. Contribution of nuisance variables to prediction.**

| | ***rho*** | | | $R^2$ | **MAE** | **BF10** | **BF01** |
|---|---|---|---|---|---|---|---|
| | M ± SE | *t* | *p* | M ± SE | M ± SE | M ± SE | M ± SE |
| *Idiographic prediction from white matter and cerebrospinal fluid signals* | | | | | | | |
| SBP | -.30 ± .04 | -7.87 | < .001 | -0.17 ± 0.04 | 3.43 ± 0.08 | 0.96 ± 0.07 | 2.64 ± 0.11 |
| HR | -.17± .04 | -4.28 | < .001 | -0.08 ± 0.04 | 2.70 ± 0.09 | 1.09 ± 0.09 | 2.52 ± 0.12 |
| *Idiographic prediction from white matter and cerebrospinal fluid signal, plus head motion estimates* | | | | | | | |
| SBP | -.10 ± .04 | -2.68 | < .001 | -0.13 ± 0.05 | 3.38 ± 0.09 | 0.51 ± 0.03 | 3.13 ± 0.10 |
| HR | -.02 ± .04 | -0.65 | .514 | -0.01 ± 0.02 | 2.61 ± 0.09 | 0.57 ± .03 | 2.87 ± 0.10 |

### 3.6.4 Predicting behavior from brain signatures of cardiovascular reactivity

Within participants, SBP and HR reactivity tended to covary with task accuracy and reaction time. Specifically, within-participant task accuracy tended to correlate negatively with SBP and HR reactivity (SBP *rho* = -.15 ± .02, $t$ = -8.71, $p$ < .001; HR *rho* = -.29 ± .02, $t$ = -14.93, $p$ < .001). Similarly, within-participant task reaction time tended to correlate positively with SBP and HR reactivity (SBP *rho* = .24 ±.02, $t$ = 9.89, $p$ < .001; HR *rho* = .32 ± .02, $t$ = 12.80, $p$ < .001). The large effects observed here may have been confounded by the presence of incongruent versus congruent conditions in the Stroop and MSIT, which were designed to experimentally affect both accuracy and reaction time between conditions (see Section 2.2.2). Thus, associations between behavioral performance and cardiovascular reactivity were reevaluated using partial correlations that adjusted for condition. These partial correlations revealed that task accuracy was not associated with cardiovascular reactivity when accounting for condition (SBP *rho* = .01 ± .02, $t$ = -1.12, $p$ = .26; HR *rho* = -.02 ± .02, $t$ = -1.13, $p$ = .25). However, task reaction time continued to correlate with cardiovascular reactivity when accounting for condition (SBP *rho* = .01 ± .02, $t$ = -1.12, $p$ = .26; HR *rho* = -.02 ± .02, $t$ = -1.13, $p$ = .25).

The generalizability of idiographic signatures and their predictions of cardiovascular reactivity as developed in Aim 1 was tested with respect to behavioral measures of task accuracy and reaction time. These analyses revealed that predicted cardiovascular reactivity tended to correlate on a within-participant basis in terms of both task accuracy and reaction time. Specifically, idiographic predictions of SBP and HR reactivity tended to generalize to predict task accuracy (SBP *rho* = -.08 ± .02, $t$ = -4.30, $p$ < .001; HR *rho* = -.11 ± .02, $t$ = -5.61, $p$ < .001). Similarly, idiographic predictions of SBP and HR reactivity tended to generalize to predict task reaction time (SBP *rho* = .18 ± .03, $t$ = 6.35, $p$ < .001; HR *rho* = .21 ± .03, $t$ = 7.46, $p$ < .001).

The associations observed between condition (incongruent, congruent), cardiovascular, and behavioral performance raised the question of whether the idiographic models using leave-one-out cross-validation may have been impacted by the presence of different conditions which reliably evoked differences in behavioral and cardiovascular responding. To this end, unplanned post-hoc analyses reran the nested cross-validated LASSO-PCR procedure described in Aim 1 but replacing the LOOCV outer fold with a k = 2 fold cross-validation outer fold and stratifying by condition. That is, models were trained on all images from one condition (e.g., incongruent, N = 8 images per participant) and tested on all images from the other condition (e.g., congruent), thus ensuring that condition-related differences in BOLD activity, behavioral performance, and/or cardiovascular reactivity did not inflate model development and testing. These idiographic models generated moderate predictions of SBP and HR reactivity (SBP *rho* = .37 ± .02, $t = 22.89$, $p < .001$; HR *rho* = .52 ± .02, $t = 31.83$, $p < .001$).

## 3.7 Exploratory post-hoc analyses

### 3.7.1 Examining sources of poor model performance

Given the above patterning of null results regarding idiographic prediction of SBP and HR reactivity, exploratory post-hoc analyses examined factors that may explain individual differences in model performance. For SBP, participants for whom the LASSO shrank all principal component features to zero showed significantly less SBP reactivity ($t = -2.22$ $p = .03$) and less SBP variability ($t$ = -2.12 p .04) than the remainder of participants but did not significantly differ in terms of baseline SBP, head motion, task accuracy, or task reaction time. For HR, participants for whom

the LASSO shrank all principal component features to zero showed significantly less HR variability ($t$ = -2.30 p .02) than the remainder of participants but did not significantly differ in terms of baseline HR, mean HR reactivity, head motion, task accuracy, or task reaction time.

Multivariable regression models examining the linear contribution to model performance (predicted-observed *rho*) by baseline cardiovascular physiology, mean reactivity, variation in reactivity, head motion, accuracy and reaction time revealed that only cardiovascular (SBP, HR) variability significantly predicted individual differences in model performance (SBP B ± SE = 0.09 ± 0.03, $t$ = 2.86, $p$ = .005; HR B ± SE = 0.08 ± 0.02, $t$ = 3.20, $p$ = .002) (Table 9). That is, the idiographic LASSO-PCR models tended to predict cardiovascular reactivity more reliably in participants who elicited more variability in their SBP and HR reactivity throughout the Stroop and MSIT. Across participants, the model performance in predicting SBP (i.e., Spearman's *rho*) was positively associated with model performance in predicting HR ($r$ = .20 $p$ = .002), suggesting that individual differences in the ability to reliably predict one measure of cardiovascular reactivity was associated with the ability to reliably predict the other.

**Table 9. Individual difference factors relating to idiographic predictions.**

Multivariable regressions examined individual differences contributing to idiographic predictions (predicted-observed Spearman's *rho*) derived in Aim 1.

| | B | SE | *t* | *p* |
|---|---|---|---|---|
| ***Idiographic SBP prediction*** | | | | |
| (Intercept) | -0.12 | 0.89 | -0.13 | .894 |
| Baseline SBP | 0.00 | 0.00 | -1.18 | .238 |
| SBP reactivity (mean) | 0.01 | 0.01 | 1.31 | .190 |
| SBP variability (SD) | 0.09 | 0.03 | 2.86 | .005 |
| Task accuracy | 0.72 | 0.85 | 0.84 | .401 |
| Task reaction time | -0.22 | 0.17 | -1.31 | .193 |
| Head motion (FD) | -0.22 | 0.37 | -0.60 | .547 |
| ***Idiographic HR prediction*** | | | | |
| (Intercept) | 0.38 | 0.77 | 0.50 | .621 |
| Baseline HR | 0.00 | 0.00 | 0.93 | .353 |
| HR reactivity (mean) | 0.01 | 0.01 | 0.58 | .563 |
| HR variability (SD) | 0.08 | 0.02 | 3.20 | .002 |
| Task accuracy | -1.04 | 0.84 | -1.24 | .217 |
| Task reaction time | -0.02 | 0.17 | -0.11 | .913 |
| Head motion (FD) | -0.53 | 0.35 | -1.50 | .135 |

### 3.7.2 Exploring alternative machine learning approaches

Multivariate signatures developed in Aim 1 performed poorly, possibly as a result of the LASSO regularization parameters shrinking all principal components to zero and producing null models (Figure 11). Hence, post-hoc exploratory analyses repeated the idiographic and other predictive models developed in Aim 1 with principal component regression (PCR). These models revealed modestly reliable predictions of SBP and HR reactivity (Figure 12; Table 10). Moreover, idiographic predictions using PCR produced significantly more reliable predictions of SBP and HR reactivity than the idiographic predictions developed in Aim 1 using LASSO-PCR (SBP *t* =

9.87, $p < .001$; HF $t = 8.77$, $p < .001$). Similarly, the cross-modal predictions applied using models developed using PCR produced significantly more reliable predictions than those from Aim 1 (SBP->HR $t = 5.30$, $p < .001$; HR->SBP $t = 2.29$, $p = .02$). By contrast, the group-based predictions using PCR did not significantly differ from those developed in Aim 1 (SBP $t = 1.51$, $p = .13$; HR $t = 1.68$, $p = .09$).

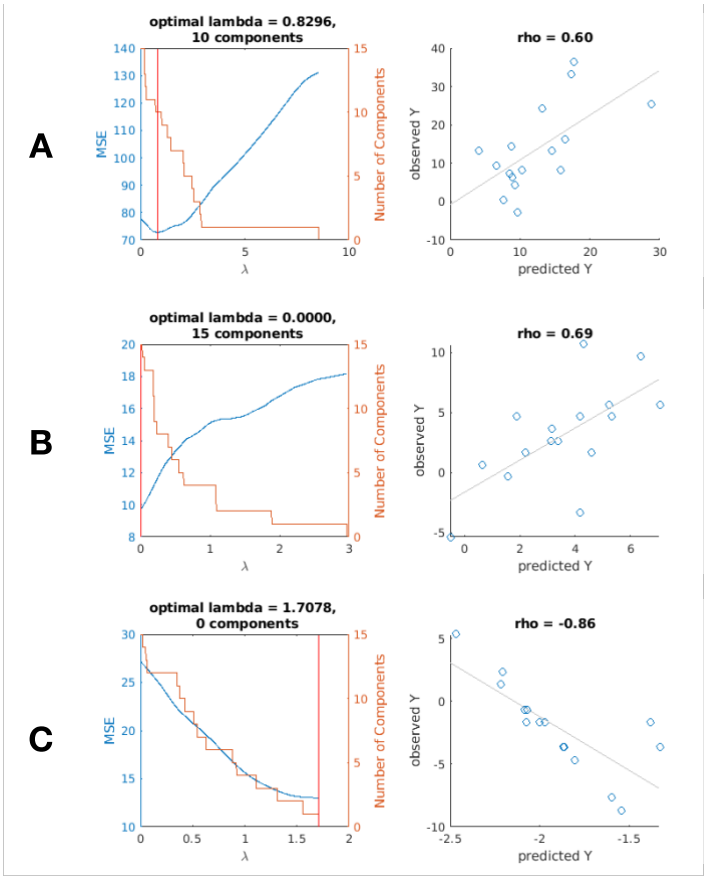


**Figure 11. Regularization within the cross-validated LASSO-PCR procedure.**

LASSO-PCR shrinks principal components of x to minimize mean square error (MSE) of cross-validated predictions. The degree of this shrinkage is determined by the parameter λ. **A.** The model that retains 10 components minimizes MSE of prediction. **B**. The model that retains all 15 components minimizes MSE of prediction, akin to principal component regression. **C**. The model that retains zero components minimizes MSE of prediction, producing a null model that predicts mean of training observations for each test observation and therefore producing a negative association between predicted and observed Y.

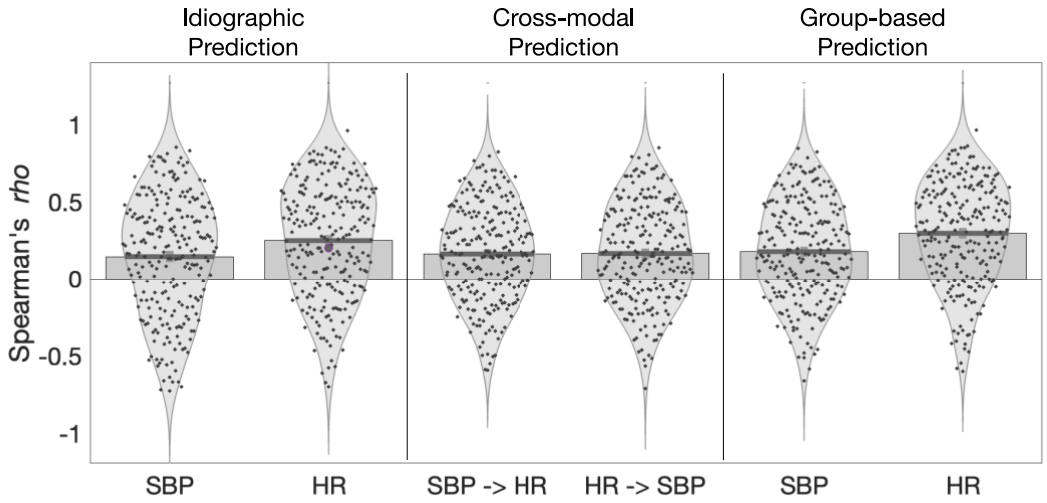


**Figure 12. Post-hoc exploratory predictions of stressor-evoked cardiovascular reactivity using principal component regression (PCR).**

Bar and violin plots depicting distributions of predictions (i.e., predicted-observed Spearman's *rho*) for multivariate signature development in post-hoc exploratory analyses using PCR. Each point depicts the prediction of a participant. Lightly shaded bars depict the group mean, and dark shaded bars reflect the group standard error (N = 242). Violin plots depict the distribution shape. Left panel describes predicted-observed associations for idiographic predictions trained to predict SBP and HR, respectively. Middle panel describes predictions trained on one measure of physiology and tested on the other. Right panel describes predictions trained using group-based cross-validation.

**Table 10. Model performance of exploratory idiographic multivariate signatures using PCR.**

Each model was evaluated according 4 sets of metrics describing the association between predicted and observed values: the Spearman's rank-order correlation (*rho*), coefficient of determination ($R^2$), mean absolute error (MAE), and Bayes Factors (BF10, BF01). Each statistic was reported using the group mean (M) and standard error (SE). In addition, the group distribution of Spearman's *rho* estimates was evaluated using a one-sample t-test.

| | ***rho*** | | | $R^2$ | **MAE** | **BF10** | **BF01** |
|---|---|---|---|---|---|---|---|
| | M ± SE | *t* | *p* | M ± SE | M ± SE | M ± SE | M ± SE |
| *Idiographic prediction* | | | | | | | |
| SBP | .14 ± .02 | 5.85 | < .001 | -0.24± 0.03 | 3.54 ± 0.09 | 0.37 ± 0.02 | 3.45 ± 0.09 |
| HR | .24 ± .02 | 10.63 | < .001 | -0.10 ± 0.03 | 2.67 ± 0.08 | 0.50 ± 0.02 | 3.28 ± 0.11 |
| *Cross-modal prediction* | | | | | | | |
| SBP -> HR | .16 ± .02 | 8.08 | < .001 | -0.67 ± 0.06 | 5.35 ± 0.22 | 0.36 ± 0.02 | 3.64 ± 0.09 |
| HR -> SBP | .10 ± .03 | 3.12 | .002 | -0.81 ± 0.28 | 5.55 ± 0.21 | 0.46 ± .03 | 3.43 ± 0.11 |
| *Group-based prediction* | | | | | | | |
| SBP | .17 ±.02 | 8.48 | < .001 | -0.63 ± 0.04 | 5.68 ± 0.22 | 0.33 ± 0.01 | 2.95 ± 0.12 |
| HR | .29 ± .02 | 13.92 | < .001 | -0.41 ± 0.04 | 6.53 ± 0.27 | 0.37 ± 0.02 | 2.43 ± 0.12 |

The model predictions using the planned LASSO-PCR method from Aim 1 and the exploratory PCR method revealed a unique patterning of associations between the two methods. This patterning is depicted in Figure 13. Specifically, in participants for whom the planned LASSO-PCR method returned a positive predicted-observed *rho*, the corresponding prediction using PCR was nearly identical (Figure 13; SBP $r$ = .95, HR $r$ = .96). However, in participants for whom the planned LASSO-PCR method returned a negative predicted-observed *rho*, the corresponding prediction using PCR was nearly always greater in magnitude (SBP: 97.0%; HR: 95.3%). This was particularly apparent in participants for whom the original LASSO-PCR model returned zero principal components via the LASSO (Figure 13, red datapoints). This suggested the apparent improvements in predictions using PCR were among participants with particularly poor

or null predictions using LASSO-PCR. Finally, comparing the unthresholded weight-maps derived from the planned LASSO-PCR and post-hoc PCR models revealed they produced highly similar maps (SBP $r$ = .85, HR $r$ = .94).

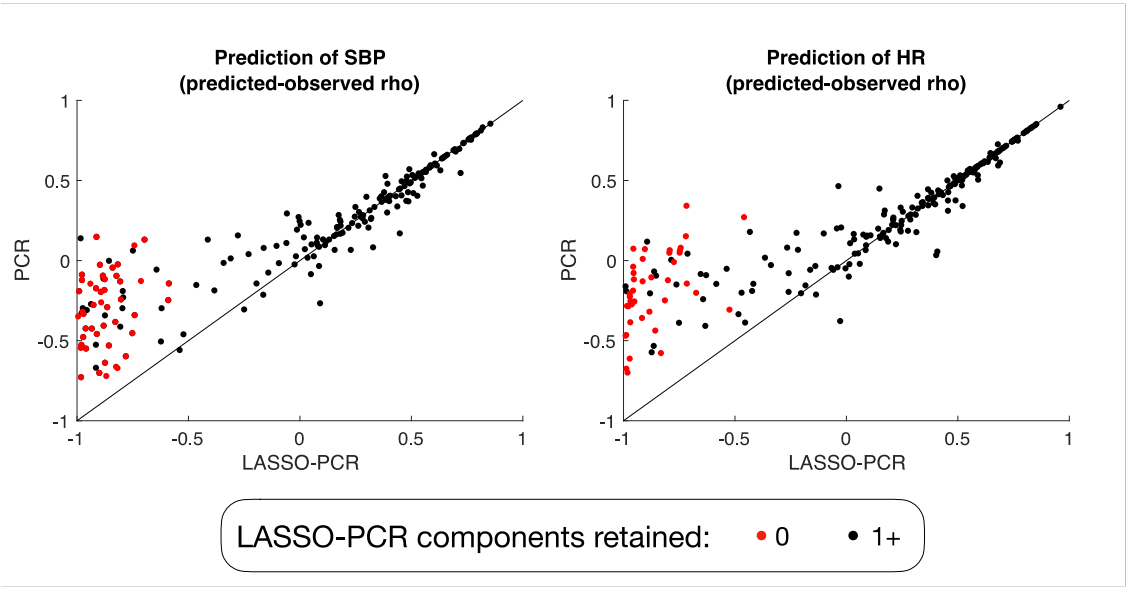


**Figure 13. Correspondence between predictions using LASSO-PCR and PCR.**

Each point depicts the predicted-observed Spearman's *rho* for a participant (N = 242). The diagonal line reflects the unity line (y = x). Colors indicate whether any principal components were retained for that participant in their LASSO-PCR idiographic model.

# 4.0 Discussion

The overarching aims of the present study were (1) to develop novel multivariate signatures of stressor-evoked brain activity that could reliably predict concurrent stressor-evoked cardiovascular reactivity within participants, and (2) to test if previously reported multivariate signatures of stressor-evoked cardiovascular reactivity could generalize to reliably predict cardiovascular physiology when tested on new participant samples, stressor contexts, and measures of cardiovascular physiology. There were 2 main sets of findings.

First, it was hypothesized that machine learning methods using dimensionality reduction, penalized regression, and cross-validation would successfully develop models and signatures of brain activity that reliably produced predictions of cardiovascular reactivity within individuals. It was also hypothesized that these signatures would generalize to predict other measures of cardiovascular reactivity as well as reactivity in other individuals. Overall, the present study found limited support for these hypotheses; that is, predictions derived from multivariate and cross-validated signatures of brain activity did not reliably correlate with within-participant changes in stressor-evoked SBP and HR activity. Moreover, these signatures did not generalize to reliably predict other measures of reactivity. However, signatures derived using group-based cross-validation showed modest predictions of reactivity. Notwithstanding their inability to reliably predict cardiovascular reactivity, however, these signatures of brain activity were found to comprise cortical and subcortical regions that are implicated in psychological stress and physiological control processes.

Second, it was hypothesized that previously published brain signatures of stressor-evoked cardiovascular reactivity would share similarities with the signatures developed in the current

study, but these published brain signatures would not generalize to reliably predict reactivity in the current study. The present study found mixed support for these hypotheses: brain signatures developed in Aim 1 were found to moderately associate with a previously published signature of HR reactivity by Eisenbarth et al. (2016), but not as strongly with a previously published signature of individual differences in SBP reactivity by Gianaros et al. (2017). Moreover, and somewhat surprisingly, the brain signature predicting individual differences in SBP reactivity by Gianaros et al. as well as the signature predicting within-participant HR reactivity were both found to modestly predict within-participant changes in SBP and HR during stress.

### 4.1 Aim 1: Multivariate signatures of stressor-evoked cardiovascular reactivity

In the present study, cross-validated multivariate signatures of stressor-evoked brain activity did not reliably predict changes in SBP and HR, contrasting with prior reports by Eisenbarth et al. (2016) and Gianaros et al. (2017). Several factors may have accounted for these differences in results, including cardiovascular monitoring methods, stressor paradigms, and the suitability of the selected machine learning algorithm; each factor is discussed below.

First, the method of cardiovascular monitoring as employed by the current study may have limited the ability to reliably predict within-participant changes in SBP and HR from stressor-evoked brain activity. To reiterate, in the present study, one SBP reading and one HR reading was collected during each 52-to-60 second incongruent and congruent block of the Stroop and MSIT. Thus, each reading of SBP and HR may have only depicted a momentary index of the prevailing SBP and HR, whereas the true SBP and HR may have significantly fluctuated throughout the block. By comparison, Eisenbarth et al. collected continuous ECG recordings and derived

continuous HR throughout the entirety of the stressor task. Thus, Eisenbarth et al. had the opportunity to characterize patterns of cardiovascular changes that may have been richer and possibly more reliable than what was collected in this sample. Future studies that aim to identify multivariate signatures of within-participant changes as attempted in the present study would likely benefit from collecting continuous measures of SBP and HR in the scanner environment.

Second, aspects of the stressor paradigm employed here may have limited or otherwise modified predictions of cardiovascular reactivity. To elaborate, the Stroop and MSIT were originally designed using principles of cardiovascular psychophysiology to measure *individual differences* in stressor-evoked cardiovascular reactivity (Kamarck & Lovallo, 2003), and were validated to reveal individual differences in brain activity showing high test-retest reliability (Sheu et al., 2012). The current study adds important new findings to this concept, specifically showing that the Stroop and MSIT employed in the MRI environment here also show acceptable internal consistency across voxels (Figure 9). Moreover, the internal consistency of individual voxels appeared to constrain their prediction weight (absolute value) in signatures of SBP and HR reactivity (Figure 10, Panel D & E). This latter observation has been reported previously in tasks involving the passive viewing of affective faces and scenes (Gianaros et al., 2020) but has not yet been explored in the Stroop and MSIT. Taken together, these findings suggest that psychometric properties such as internal consistency may significantly influence multivariate brain imaging signatures.

However, despite the acceptable psychometric properties (i.e., test-retest reliability, internal consistency) of the Stroop and MSIT, it is possible that these tasks may not have elicited sufficient *variability* in SBP or HR to enable reliable predictions on a within-participant basis. Evidence for this possibility comes from post-hoc analyses showing that greater *variability* in SBP

and HR during the stressor tasks was associated with improved predictions in idiographic models (Table 9). As the primary models used idiographic cross-validation, it follows that models would require a sufficient level of variation in the outcome (e.g., SBP) in order to identify and validate reliable predictors. By contrast, models trained on outcomes with little or no variability would overfit the training data, thus capturing noise or measurement error in the outcome and not reliably predicting outcomes in holdout test data. Hence, it is possible that although the Stroop and MSIT elicited robust changes in overall SBP and HR (see Figure 1) that makes them well-suited to the study of individual differences, they may not have elicited sufficient variability in SBP and HR to identify predictors of changes within participants. As a comparison, in the speech preparation task employed by Eisenbarth et al., there may have been greater variability in changes on a within-participant basis, because the psychological demands of having to give a speech evolves slowly throughout the scan session.

Another aspect of the task paradigm that may have influenced predictions involves the use of different conditions (i.e., incongruent, congruent) that systematically engage varying levels of psychological experiences, behavioral responses, and cardiovascular reactivity. As described previously, due to their design, the incongruent and congruent conditions of the Stroop and MSIT reliably differ in terms of response accuracy and reaction time. In addition to their well-documented differences in brain activity (Figure 1; Gianaros et al., 2017; Sheu et al., 2012), these tasks elicited condition-related differences in SBP and HR in the analytic sample (Section 3.2). Hence, it is possible that the presence of strong condition-related effects may have obscured the multivariate relationship between patterns of brain activity and prevailing cardiovascular reactivity. This possibility was examined by conducting post-hoc analyses that cross-validated predictions within each condition separately. The models derived from these analyses showed

moderate prediction of SBP and HR (Section 3.6.4), thus suggesting that conditions may not have systematically influenced prediction in the primary analyses.

A third factor possibly contributing to the results may have been related to the selection of dimensionality reduction and regularized regression methods. To this point, violin plots depicting the distribution of idiographic predictions revealed that, for both SBP and HR, a substantial proportion of idiographic models returned a prediction-observed Spearman's *rho* with a large negative effect size (e.g., *rho* < -.75), as evidenced by the heavy lower tail in both distributions (Figure 3, left panel). Notably, the predictions generated by the group-based prediction did not show this heavy lower tail (Figure 3, right panel). Examining idiographic models with large negative predictions revealed that, for many participants, the poor model fit may have been attributable to the cross-validated LASSO regularization procedure. To elaborate, the LASSO regularization procedure optimized the shrinkage parameter λ in order to minimize the MSE of predictions (Figure 11, left panels, blue lines). In many participants, the minimum MSE was obtained via cross-validation to retain either some (Figure 11A) or all (Figure 11B) principal components. The latter model is identical to principal components regression. However, in some idiographic models, the level of λ producing the minimum MSE required shrinking all principal components to zero (Figure 11C), thus producing returning a so-called 'null' model comprising zero voxel weights and a constant term. Thus, for these idiographic models, the cross-validated predictions of test observations comprised the mean value of all training observations in that cross-validation fold, which therefore produced a negative correlation between test observations and test predictions across leave-one-out cross-validation folds (Figure 11C).

The negative predictions produced above raised the question of whether the LASSO regression step of the LASSO-PCR algorithm produced biased predictions in the context of null

or otherwise small effect sizes. To explore this, post-hoc exploratory analyses conducted permutation tests to characterize the null distribution of effect sizes produced by LASSO-PCR (Coutanche & Hallion, 2019). Specifically, in 1000 participants selected with replacement, cardiovascular reactivity scores (SBP or HR) were permuted, and idiographic models were developed to predict these permuted scores. These permutation analyses showed that the idiographic prediction of permuted SBP and HR was *rho* = -.45 ± .02, $t$ = -29.02, $p < .001$, and *rho* = -.40 ± .02, $t$ = -25.43, $p < .001$, respectively. Thus, when attempting to predict permuted data, the LASSO-PCR procedure produces negatively biased predictions that are not centered around *rho* = 0. By contrast, predictions of permuted reactivity that were derived from previously published multivariate signatures were found to produce null distributions that center around *rho* = 0 (range .002 to .007; $p$'s > .42). Thus, the LASSO-PCR procedure may be produced negatively biased predictions in the context of null or low effect sizes as observed in the present study.

To test if the regularized regression step of the LASSO-PCR procedure was indeed implicated in producing poor model fits, in a set of post-hoc exploratory analyses, idiographic cross-validated predictions were repeated using principal components regression (PCR) without regularized regression via the LASSO. PCR produced relatively reliable predictions of SBP and HR reactivity (Table 10; Figure 12) and these predictions were significantly improved over the *a priori* LASSO-PCR models. Importantly, whereas PCR offered little improvement over LASSO-PCR for models with positive predictions, PCR offered substantial improvement over LASSO-PCR for models with negative predictions (rho < 0), especially models that retained zero principal components in regularized regression (Figure 13, red points).

Another potential reason why the selection of regularized regression approaches may not have fit the present study was due to the number of observations (n) and features (p) available in

each model. First, because there were 16 block-related measures of SBP and HR reactivity per participant, idiographic models using leave-one-out cross-validation in the present study could not create training folds comprising more than 15 images. By comparison, the study by Eisenbarth et al. cross-validated models using 80 training images and 11 test images in each fold, thus potentially providing more stable predictions across cross-validation folds that would therefore more likely generalize to new test data and test individuals (Woo et al., 2017). Moreover, because the LASSO-PCR routine used a principal component reduction step prior to the LASSO, the feature space was reduced from > 200,000 voxels to p = n-1 (i.e., 15) principal components. Thus, the number of principal component features available to fit in cross-validated idiographic models may have been too small to reliably predict reactivity. As stated previously, measuring cardiovascular reactivity at a higher temporal resolution has the potential to side-step this issue in future studies.

In addition to the above factors, there was a possibility that factors such as physiological noise or head motion may have confounded multivariate predictions of cardiovascular reactivity, especially considering the dramatic effect these nuisance variables have on metrics of functional connectivity MRI (Power et al., 2012; Satterthwaite et al., 2012). However, multivariate predictions using these variables failed to reliably predict SBP and HR reactivity (Table 8), and moreover the prediction of HR reactivity was significantly worse than the primary idiographic models, indicating that it was unlikely that these factors had a significant confounding influence on the results obtained in the primary analyses.

As expected, because idiographic models generated unreliable predictions of SBP reactivity, they subsequently did not generalize to predict HR reactivity (Figure 3; Table 2). However, and somewhat surprisingly, idiographic models trained to predict HR appeared to modestly predict SBP reactivity (Table 2), although it should be noted that most individual

predictions were not significant. Moreover, and in contrast to the findings by Eisenbarth et al., group-based models produced improved predictions over idiographic models for both SBP and HR reactivity. However, this conflicting finding was most likely due to the poor performance of the idiographic models, as the predictions from the group-based models explored here were somewhat smaller in effect size than the group-based predictions reported by Eisenbarth et al. ($r$ = .32). Nonetheless, these findings confirm prior findings that individuals share commonalities in terms of brain representations of cardiovascular reactivity during stress.

Notwithstanding the above problems with generating reliable predictions of stressor-evoked cardiovascular reactivity, the models generated brain signatures that comprised key visceral control circuits that have long been implicated in psychological stress and cardiovascular control. Most notably, when applying an FDR correction to the brain signatures for SBP reactivity, the dACC emerged as a consistent contributor to (albeit unreliable) predictions. The dACC is functionally implicated in numerous psychological processes, including cognitive control, error monitoring, action selection, negative emotion, threat processing, and pain processing (Botvinick et al., 2004; Kragel et al., 2018; Shackman et al., 2011; Shenhav et al., 2016; Wager et al., 2016). Moreover, the ACC is broadly implicated in regulating peripheral cardiovascular physiology via its direct connections to autonomic and neuroendocrine effector pathways (Amiez & Procyk, 2019; Dum et al., 2016; B. Vogt, 2009). As detailed previously, the dorsal subdivision of the ACC in particular is commonly associated with pro-sympathetic influences over the ANS, which may become particularly apparent in the context of behaviorally-evoked cardiovascular reactivity (Critchley, 2004; Gianaros & Wager, 2015); (Matthews et al., 2004; Thayer & Lane, 2009). For example, patients with lesions to the dACC show reduced BP and HR responses to psychological and physical stressors (Critchley et al., 2003), and electrically stimulating the dACC in epilepsy

patients induces transient increases in BP and HR (Caruana et al., 2018; Parvizi et al., 2013; Pool & Ransohoff, 1949). Thus, the present study contributes to the growing body of evidence suggesting the dACC may comprise a key cortical regulator of SBP, particularly in the context of psychological stress.

The brain signature of HR reactivity comprised weights in several hypothesized brain regions, including the vmPFC, amygdala, and hippocampus. The negative weights in the vmPFC are consistent with several studies showing negative associations between vmPFC activity and HR reactivity, consistent with a hypothesized role for the vmPFC in pro-parasympathetic outflow (Gianaros et al., 2004; Matthews et al., 2004; Thayer et al., 2012; Wager, Waugh, et al., 2009). The negative weights in the amygdala and hippocampus are somewhat consistent with other studies reporting stressor-evoked deactivation in limbic structures (Pruessner et al., 2008), although the directionality of the association between amygdala activity and HR reactivity have been mixed (Critchley et al., 2000; Wager, Waugh, et al., 2009). Finally, negative weights were observed in the bilateral posterior insula, a region which is implicated in processing ascending viscerosensory information (Craig, 2009, 2014).

The brain signatures trained to predict SBP and HR reactivity were correlated both at the whole-brain and at the local pattern level, and moreover did not show significant differences in prediction weights at the voxel level. This suggests these two signatures may be capturing substantial shared variance in cardiovascular reactivity suggesting these two models may be capturing substantial shared variance. This finding contrasts somewhat with the results of Eisenbarth et al., who observed several differences in multivariate signatures of HR and skin conductance level (SCL) reactivity. Although there were no statistically significant differences between the SBP and HR signatures at the voxel-wise level, network analyses showed significant

differences in how these signatures were represented within large-scale intrinsic networks. Chief among these differences were significantly more negative correspondence of the HR signature with the somatomor, limbic and default mode networks. These differences between signatures at the network level suggest that even evaluating and comparing multivariate signatures may require pattern-based approaches, as opposed to voxel-wise statistical tests (Ginty et al., 2019)

### 4.2 Aim 2: Generalizability of published multivariate signatures

In the present study, comparing the empirically derived idiographic maps with previously published signatures revealed associations with the signature of Eisenbarth et al. (2016). Specifically, the voxel-wise HR reactivity pattern was positively associated with the signature of Eisenbarth et al., and moreover shared several commonalities, including positive weights in the dACC, DLPFC, and cerebellum, as well as negative weights in the vmPFC, temporal lobe, and posterior insula. It should be noted that these associations were observed despite the two studies differing appreciably in terms of their participant demographics and stressor paradigm. It may be speculated that these strong associations may have been related to their shared capturing of within-person changes in cardiovascular physiology, as opposed to stable individual differences as captured by Gianaros et al. (2017). By contrast, the signature of SBP reactivity shared commonalities with the signature by Gianaros et al. via positive weights in the dACC, again suggesting this region may be implicated in translating both within-participant processes related to SBP changes as well as the expression of individual differences in SBP reactivity.

Previously published brain signatures of stressor-evoked cardiovascular reactivity were found to modestly predict SBP and HR responses during stress in the analytic sample. To my

knowledge, this was the first study to empirically test the generalizability of brain signatures in this domain. Such generalizability tests have been widely conducted in other areas of research, including pain processing (Wager et al., 2013), negative emotion (Sicorello et al., 2021), and decision making (Cosme et al., 2020). However, the effect sizes observed in this aim, while statistically significant, were substantially smaller in magnitude than the effects observed in the above fields pertaining to generalizability of predictions. Nonetheless, these tests comprise a critical step towards building a repertoire of brain signatures that reflect various aspects and contexts of stress-related physiology that are important for health (Erickson et al., 2014; Inagaki, 2020).

### 4.3 Strengths

The present study had several strengths, including the use of a representative sample of healthy adults free of potentially confounding chronic physical disease or medication use that may have affected cardiovascular physiology. Second, the use of multivariate and machine learning approaches to predict stressor-evoked cardiovascular reactivity represents an important departure from mass-univariate correlational approaches that are subject to elevated false positive rates and poor generalizability (Eklund et al., 2016; Kriegeskorte et al., 2009). Third, the second aim utilized what could be considered a so-called ‘gold-standard’ approach of cross-validating multivariate brain signatures of a psychological or behavioral process across studies – that is, taking a model trained in a different sample and applying it to a novel context and set of participants (Scheinost et al., 2019). Finally, this study also carefully considered the psychometric properties of the brain

imaging data, which are becoming more important in the context of developing reliable models of psychological processes by brain imaging data (Kragel et al., 2021).

## 4.4 Limitations

In addition to the previously detailed limitations regarding cardiovascular monitoring method and task design, it should be noted that the predictions explored in this study are nonetheless cross-sectional in nature. In other words, although the signatures developed here and in other studies were used to 'predict' measures of cardiovascular reactivity, they do not demonstrate that patterns of stressor-evoked brain responses have a causal influence over cardiovascular reactivity. Indeed, patterns or features of stressor-evoked brain activity may reflect efferent visceromotor commands to influence peripheral cardiovascular physiology, or they may reflect ongoing viscerosensory processing or representation of the prevailing or changing cardiovascular physiology in the periphery, or they may reflect some combination of the two mechanisms (Kraynak et al., in prep; Seeley, 2019). To address this limitation, future studies will need to combine the multivariate methods used in this study with study designs that experimentally manipulate brain activity (e.g., using noninvasive neuromodulation; Kaur et al., 2020; Makovac et al., 2017) or modulate peripheral cardiovascular physiology (e.g., using physiological challenges; Hassanpour et al., 2016) and test for effects and predictions on subsequent responses to psychological stressors .

## 4.5 Future directions

As mentioned previously, future studies could aim to replicate and extend these findings by employing more fine-grained measurement of SBP and HR during stressor paradigms. Moreover, future studies might incorporate multilevel modeling into the above machine learning and cross validation methods in novel participants to better parse components of brain activity that reliably contribute to within-person changes versus stable individual differences (Petre et al., 2019). Further exploring these multivariate signatures will increase our understanding of the brain systems that may link psychological stress to CVR risk.

## 4.6 Conclusions

In summary, the present study aimed to build upon the small but growing number of brain imaging studies using machine learning methods to predict stressor-evoked cardiovascular reactivity, a known biobehavioral risk marker for CVD. The findings of the study suggest that stressor-evoked cardiovascular reactivity may not always be reliably predicted by patterns of brain activity, depending on the stressor task and the parameters of cardiovascular physiology. This study adds preliminary evidence that cross-validated models of stressor-evoked cardiovascular reactivity may moderately generalize to participant samples and stressor paradigms, which is a critical validation step toward developing brain-based signatures of stress-related disease risk that may be eventually used identify at-risk individual or identify treatment targets.

## Bibliography


Akdeniz, C., Tost, H., Streit, F., Haddad, L., Wüst, S., Schäfer, A., Schneider, M., Rietschel, M., Kirsch, P., & Meyer-Lindenberg, A. (2014). Neuroimaging evidence for a role of neural social stress processing in ethnic minority-associated environmental risk. *JAMA Psychiatry, 71*(6), 672–680. https://doi.org/10.1001/jamapsychiatry.2014.35

Allen, M. T., Boquet, A. J., & Shelley, K. S. (1991). Cluster analyses of cardiovascular responsivity to three laboratory stressors. *Psychosomatic Medicine, 53*(3), 272–288. https://doi.org/10.1097/00006842-199105000-00002

Allen, M. T., & Crowell, M. D. (1989). Patterns of Autonomic Response During Laboratory Stressors. *Psychophysiology, 26*(5), 603–614. https://doi.org/10.1111/j.1469-8986.1989.tb00718.x

Amiez, C., & Procyk, E. (2019). Chapter 4—Midcingulate somatomotor and autonomic functions. In B. A. Vogt (Ed.), *Handbook of Clinical Neurology* (Vol. 166, pp. 53–71). Elsevier. https://doi.org/10.1016/B978-0-444-64196-0.00004-2

Bairey Merz, C. N., Dwyer, J., Nordstrom, C. K., Walton, K. G., Salerno, J. W., & Schneider, R. H. (2002). Psychosocial Stress and Cardiovascular Disease: Pathophysiological Links. *Behavioral Medicine (Washington, D.C.), 27*(4), 141–147.

Beissner, F., Meissner, K., Bär, K.-J., & Napadow, V. (2013). The autonomic brain: An activation likelihood estimation meta-analysis for central processing of autonomic function. *The Journal of Neuroscience: The Official Journal of the Society for Neuroscience, 33*(25), 10503–10511. https://doi.org/10.1523/JNEUROSCI.1103-13.2013

Benjamini, Y., & Hochberg, Y. (1995). Controlling the false discovery rate: A practical and powerful approach to multiple testing. *Journal of the Royal Statistical Society. Series B (Methodological)*, *57*(1), 289–300.

Berntson, G. G., & Cacioppo, J. T. (2007). Integrative physiology: Homeostasis, allostasis and the orchestration of systemic physiology. *Handbook of Psychophysiology*, *3*, 433–452.

Berntson, G. G., Cacioppo, J. T., Binkley, P. F., Uchino, B. N., Quigley, K. S., & Fieldstone, A. (1994). Autonomic cardiac control. III. Psychological stress and cardiac response in autonomic space as revealed by pharmacological blockades. *Psychophysiology*, *31*(6), 599–608. https://doi.org/10.1111/j.1469-8986.1994.tb02352.x

Botvinick, M. M., Cohen, J. D., & Carter, C. S. (2004). Conflict monitoring and anterior cingulate cortex: An update. *Trends in Cognitive Sciences*, *8*(12), 539–546. https://doi.org/10.1016/j.tics.2004.10.003

Boutcher, Y. N., & Boutcher, S. H. (2006). Cardiovascular response to Stroop: Effect of verbal response and task difficulty. *Biological Psychology*, *73*(3), 235–241. https://doi.org/10.1016/j.biopsycho.2006.04.005

Brindle, R. C., Ginty, A. T., Phillips, A. C., & Carroll, D. (2014). A tale of two mechanisms: A meta-analytic approach toward understanding the autonomic basis of cardiovascular reactivity to acute psychological stress. *Psychophysiology*, *51*(10), 964–976. https://doi.org/10.1111/psyp.12248

Bush, G., & Shin, L. M. (2006). The Multi-Source Interference Task: An fMRI task that reliably activates the cingulo-frontal-parietal cognitive/attention network. *Nature Protocols*, *1*(1), 308–313. https://doi.org/10.1038/nprot.2006.48

Carroll, D., Phillips, A. C., & Balanos, G. M. (2009). Metabolically exaggerated cardiac reactions to acute psychological stress revisited. *Psychophysiology*, *46*(2), 270–275. https://doi.org/10.1111/j.1469-8986.2008.00762.x

Caruana, F., Gerbella, M., Avanzini, P., Gozzo, F., Pelliccia, V., Mai, R., Abdollahi, R. O., Cardinale, F., Sartori, I., Lo Russo, G., & Rizzolatti, G. (2018). Motor and emotional behaviours elicited by electrical stimulation of the human cingulate cortex. *Brain*, *141*(10), 3035–3051. https://doi.org/10.1093/brain/awy219

Chida, Y., & Steptoe, A. (2010). Greater Cardiovascular Responses to Laboratory Mental Stress Are Associated With Poor Subsequent Cardiovascular Risk Status A Meta-Analysis of Prospective Evidence. *Hypertension*, *55*(4), 1026–1032. https://doi.org/10.1161/HYPERTENSIONAHA.109.146621

Cicchetti, D. V. (1994). Guidelines, criteria, and rules of thumb for evaluating normed and standardized assessment instruments in psychology. *Psychological Assessment, 6*(4), 284–290. https://doi.org/10.1037/1040-3590.6.4.284

Ciric, R., Wolf, D. H., Power, J. D., Roalf, D. R., Baum, G. L., Ruparel, K., Shinohara, R. T., Elliott, M. A., Eickhoff, S. B., Davatzikos, C., Gur, R. C., Gur, R. E., Bassett, D. S., & Satterthwaite, T. D. (2017). Benchmarking of participant-level confound regression strategies for the control of motion artifact in studies of functional connectivity. *NeuroImage*, *154*, 174–187. https://doi.org/10.1016/j.neuroimage.2017.03.020

Cohen, S., Gianaros, P. J., & Manuck, S. B. (2016). A Stage Model of Stress and Disease. *Perspectives on Psychological Science: A Journal of the Association for Psychological Science*, *11*(4), 456–463. https://doi.org/10.1177/1745691616646305

Cosme, D., Zeithamova, D., Stice, E., & Berkman, E. T. (2020). Multivariate neural signatures for health neuroscience: Assessing spontaneous regulation during food choice. *Social Cognitive and Affective Neuroscience*, *15*(10), 1120–1134. https://doi.org/10.1093/scan/nsaa002

Coutanche, M. N., & Hallion, L. S. (2019). *Machine Learning for Clinical Psychology and Clinical Neuroscience*. PsyArXiv. https://doi.org/10.31234/osf.io/7zswh

Craig, A. D. (2009). How do you feel — now? The anterior insula and human awareness. *Nature Reviews Neuroscience*, *10*(1), 59–70. https://doi.org/10.1038/nrn2555

Craig, A. D. (2014). Topographically organized projection to posterior insular cortex from the posterior portion of the ventral medial nucleus in the long-tailed macaque monkey. *The Journal of Comparative Neurology*, *522*(1), 36–63. https://doi.org/10.1002/cne.23425

Critchley, H. D. (2004). The human cortex responds to an interoceptive challenge. *Proceedings of the National Academy of Sciences of the United States of America*, *101*(17), 6333–6334. https://doi.org/10.1073/pnas.0401510101

Critchley, H. D., Corfield, D. R., Chandler, M. P., Mathias, C. J., & Dolan, R. J. (2000). Cerebral correlates of autonomic cardiovascular arousal: A functional neuroimaging investigation in humans. *The Journal of Physiology*, *523*(Pt 1), 259–270. https://doi.org/10.1111/j.1469-7793.2000.t01-1-00259.x

Critchley, H. D., Mathias, C. J., Josephs, O., O'Doherty, J., Zanini, S., Dewar, B.-K., Cipolotti, L., Shallice, T., & Dolan, R. J. (2003). Human cingulate cortex and autonomic control: Converging neuroimaging and clinical evidence. *Brain*, *126*(10), 2139–2152. https://doi.org/10.1093/brain/awg216

Damasio, A., & Carvalho, G. B. (2013). The nature of feelings: Evolutionary and neurobiological origins. *Nature Reviews Neuroscience*, *14*(2), 143–152. https://doi.org/10.1038/nrn3403

Davis, M., & Whalen, P. J. (2001). The amygdala: Vigilance and emotion. *Molecular Psychiatry*, *6*(1), 13–34. https://doi.org/10.1038/sj.mp.4000812

Debski, T. T., Kamarck, T. W., Richard Jennings, J., Young, L. W., Eddy, M. J., & Zhang, Y. (1991). A computerized test battery for the assessment of cardiovascular reactivity. *International Journal of Bio-Medical Computing*, *27*(3–4), 277–289. https://doi.org/10.1016/0020-7101(91)90068-P

Dedovic, K., Renwick, R., Mahani, N. K., Engert, V., Lupien, S. J., & Pruessner, J. C. (2005). The Montreal Imaging Stress Task: Using functional imaging to investigate the effects of perceiving and processing psychosocial stress in the human brain. *Journal of Psychiatry and Neuroscience*, *30*(5), 319–325.

Dum, R. P., Levinthal, D. J., & Strick, P. L. (2016). Motor, cognitive, and affective areas of the cerebral cortex influence the adrenal medulla. *Proceedings of the National Academy of Sciences*, *113*(35), 9922–9927. https://doi.org/10.1073/pnas.1605044113

Efron, B., Hastie, T., Johnstone, I., & Tibshirani, R. (2004). Least angle regression. *Annals of Statistics*, *32*(2), 407–499. https://doi.org/10.1214/009053604000000067

Eisenbarth, H., Chang, L. J., & Wager, T. D. (2016). Multivariate brain prediction of heart rate and skin conductance responses to social threat. *Journal of Neuroscience*, *36*(47), 11987–11998. https://doi.org/10.1523/JNEUROSCI.3672-15.2016

Eklund, A., Nichols, T. E., & Knutsson, H. (2016). Cluster failure: Why fMRI inferences for spatial extent have inflated false-positive rates. *Proceedings of the National Academy of Sciences*, *113*(28), 7900–7905. https://doi.org/10.1073/pnas.1602413113

Elliott, M. L., Knodt, A. R., Ireland, D., Morris, M. L., Poulton, R., Ramrakha, S., Sison, M. L., Moffitt, T. E., Caspi, A., & Hariri, A. R. (2020). What Is the Test-Retest Reliability of Common Task-Functional MRI Measures? New Empirical Evidence and a Meta-Analysis. *Psychological Science*, *31*(7), 792–806. https://doi.org/10.1177/0956797620916786

Erickson, K. I., Creswell, J. D., Verstynen, T. D., & Gianaros, P. J. (2014). Health Neuroscience Defining a New Field. *Current Directions in Psychological Science*, *23*(6), 446–453. https://doi.org/10.1177/0963721414549350

Fechir, M., Gamer, M., Blasius, I., Bauermann, T., Breimhorst, M., Schlindwein, P., Schlereth, T., & Birklein, F. (2010). Functional imaging of sympathetic activation during mental stress. *NeuroImage*, *50*(2), 847–854. https://doi.org/10.1016/j.neuroimage.2009.12.004

Folkman, S., Lazarus, R. S., Dunkel-Schetter, C., DeLongis, A., & Gruen, R. J. (1986). Dynamics of a stressful encounter: Cognitive appraisal, coping, and encounter outcomes. *Journal of Personality and Social Psychology*, *50*(5), 992–1003.

Folkman, S., Lazarus, R. S., Gruen, R. J., & DeLongis, A. (1986). Appraisal, coping, health status, and psychological symptoms. *Journal of Personality and Social Psychology*, *50*(3), 571–579.

Forman, G., & Scholz, M. (2010). Apples-to-apples in cross-validation studies: Pitfalls in classifier performance measurement. *ACM SIGKDD Explorations Newsletter*, *12*(1), 49–57. https://doi.org/10.1145/1882471.1882479

Gianaros, P. J., Bleil, M. E., Muldoon, M. F., Jennings, J. R., Sutton-Tyrrell, K., McCaffery, J. M., & Manuck, S. B. (2002). Is cardiovascular reactivity associated with atherosclerosis among hypertensives? *Hypertension (Dallas, Tex.: 1979)*, *40*(5), 742–747. https://doi.org/10.1161/01.hyp.0000035707.57492.eb

Gianaros, P. J., Derbtshire, S. W. G., May, J. C., Siegle, G. J., Gamalo, M. A., & Jennings, J. R. (2005). Anterior cingulate activity correlates with blood pressure during stress. *Psychophysiology*, *42*(6), 627–635. https://doi.org/10.1111/j.1469-8986.2005.00366.x

Gianaros, P. J., & Jennings, J. R. (2018). Host in the machine: A neurobiological perspective on psychological stress and cardiovascular disease. *American Psychologist*, *73*(8), 1031–1044. https://doi.org/10.1037/amp0000232

Gianaros, P. J., Kraynak, T. E., Kuan, D. C.-H., Gross, J. J., McRae, K., Hariri, A. R., Manuck, S. B., Rasero, J., & Verstynen, T. D. (2020). Affective brain patterns as multivariate neural correlates of cardiovascular disease risk. *Social Cognitive and Affective Neuroscience*, *15*(10), 1034–1045. https://doi.org/10.1093/scan/nsaa050

Gianaros, P. J., & Sheu, L. K. (2009). A review of neuroimaging studies of stressor-evoked blood pressure reactivity: Emerging evidence for a brain-body pathway to coronary heart disease risk. *NeuroImage*, *47*(3), 922–936. https://doi.org/10.1016/j.neuroimage.2009.04.073

Gianaros, P. J., Sheu, L. K., Matthews, K. A., Jennings, J. R., Manuck, S. B., & Hariri, A. R. (2008). Individual Differences in Stressor-Evoked Blood Pressure Reactivity Vary with Activation, Volume, and Functional Connectivity of the Amygdala. *The Journal of Neuroscience*, *28*(4), 990–999. https://doi.org/10.1523/JNEUROSCI.3606-07.2008

Gianaros, P. J., Sheu, L. K., Uyar, F., Koushik, J., Jennings, J. R., Wager, T. D., Singh, A., & Verstynen, T. D. (2017). A brain phenotype for stressor-evoked blood pressure reactivity. *Journal of the American Heart Association*, *6*(9), e006053. https://doi.org/10.1161/JAHA.117.006053

Gianaros, P. J., Van der Veen, F. M., & Jennings, J. R. (2004). Regional cerebral blood flow correlates with heart period and high-frequency heart period variability during working-

memory tasks: Implications for the cortical and subcortical regulation of cardiac autonomic activity. *Psychophysiology*, *41*(4), 521–530. https://doi.org/10.1111/1469-8986.2004.00179.x

Gianaros, P. J., & Wager, T. D. (2015). Brain-body pathways linking psychological stress and physical health. *Current Directions in Psychological Science*, *24*(4), 313–321. https://doi.org/10.1177/0963721415581476

Ginty, A. T., Kraynak, T. E., Kuan, D. C., & Gianaros, P. J. (2019). Ventromedial prefrontal cortex connectivity during and after psychological stress in women. *Psychophysiology*, e13445. https://doi.org/10.1111/psyp.13445

Goldstein, L. E., Rasmusson, A. M., Bunney, B. S., & Roth, R. H. (1996). Role of the Amygdala in the Coordination of Behavioral, Neuroendocrine, and Prefrontal Cortical Monoamine Responses to Psychological Stress in the Rat. *Journal of Neuroscience*, *16*(15), 4787–4798. https://doi.org/10.1523/JNEUROSCI.16-15-04787.1996

Gordan, R., Gwathmey, J. K., & Xie, L.-H. (2015). Autonomic and endocrine control of cardiovascular function. *World Journal of Cardiology*, *7*(4), 204–214. https://doi.org/10.4330/wjc.v7.i4.204

Gorgolewski, K. J., Varoquaux, G., Rivera, G., Schwarz, Y., Ghosh, S. S., Maumet, C., Sochat, V. V., Nichols, T. E., Poldrack, R. A., Poline, J.-B., Yarkoni, T., & Margulies, D. S. (2015). NeuroVault.org: A web-based repository for collecting and sharing unthresholded statistical maps of the human brain. *Frontiers in Neuroinformatics*, *9*. https://doi.org/10.3389/fninf.2015.00008

Grossman, P., Watkins, L. L., Wilhelm, F. H., Manolakis, D., & Lown, B. (1996). Cardiac vagal control and dynamic responses to psychological stress among patients with coronary artery

disease. *The American Journal of Cardiology*, *78*(12), 1424–1427. https://doi.org/10.1016/S0002-9149(97)89295-8

Hall, J. E. (2015). *Guyton and Hall Textbook of Medical Physiology* (13th edition). Saunders.

Hassanpour, M. S., Yan Lirong, Wang Danny J. J., Lapidus Rachel C., Arevian Armen C., Simmons W. Kyle, Feusner Jamie D., & Khalsa Sahib S. (2016). How the heart speaks to the brain: Neural activity during cardiorespiratory interoceptive stimulation. *Philosophical Transactions of the Royal Society B: Biological Sciences*, *371*(1708), 20160017. https://doi.org/10.1098/rstb.2016.0017

Hastie, T., Tibshirani, R., & Friedman, J. (2009). *The Elements of Statistical Learning: Data Mining, Inference, and Prediction, Second Edition*. Springer Science & Business Media.

Haxby, J. V., Gobbini, M. I., Furey, M. L., Ishai, A., Schouten, J. L., & Pietrini, P. (2001). Distributed and Overlapping Representations of Faces and Objects in Ventral Temporal Cortex. *Science*, *293*(5539), 2425–2430. https://doi.org/10.1126/science.1063736

Hess, W. R., & Brügger, M. (1943). Das subkortikale Zentrum der affektiven Abwehrreaktion. *Helvetica Physiologica et Pharmacologica Acta*.

Inagaki, T. K. (2020). Health neuroscience 2.0: Integration with social, cognitive and affective neuroscience. *Social Cognitive and Affective Neuroscience*, *15*(10), 1017–1023. https://doi.org/10.1093/scan/nsaa123

Infantolino, Z. P., Luking, K. R., Sauder, C. L., Curtin, J. J., & Hajcak, G. (2018). Robust is not necessarily reliable: From within-subjects fMRI contrasts to between-subjects comparisons. *NeuroImage*, *173*, 146–152. https://doi.org/10.1016/j.neuroimage.2018.02.024

Jennings, J. R., Kamarck, T. W., Everson-Rose, S. A., Kaplan, G. A., Manuck, S. B., & Salonen, J. T. (2004). Exaggerated blood pressure responses during mental stress are prospectively related to enhanced carotid atherosclerosis in middle-aged Finnish men. *Circulation*, *110*(15), 2198–2203. https://doi.org/10.1161/01.CIR.0000143840.77061.E9

Kamarck, T. W., Everson, S. A., Kaplan, G. A., Manuck, S. B., Jennings, J. R., Salonen, R., & Salonen, J. T. (1997). Exaggerated Blood Pressure Responses During Mental Stress Are Associated With Enhanced Carotid Atherosclerosis in Middle-Aged Finnish Men: Findings From the Kuopio Ischemic Heart Disease Study. *Circulation*, *96*(11), 3842–3848. https://doi.org/10.1161/01.CIR.96.11.3842

Kamarck, T. W., Jennings, J. R., Debski, T. T., Glickman-Weiss, E., Johnson, P. S., Eddy, M. J., & Manuck, S. B. (1992). Reliable Measures of Behaviorally-Evoked Cardiovascular Reactivity from a PC-Based Test Battery: Results from Student and Community Samples. *Psychophysiology*, *29*(1), 17–28. https://doi.org/10.1111/j.1469-8986.1992.tb02006.x

Kamarck, T. W., Jennings, J. R., Pogue-Geile, M., & Manuck, S. B. (1994). A multidimensional measurement model for cardiovascular reactivity: Stability and cross-validation in two adult samples. *Health Psychology*, *13*(6), 471–478. https://doi.org/10.1037/0278-6133.13.6.471

Kamarck, T. W., Li, X., Wright, A. G. C., Muldoon, M. F., & Manuck, S. B. (2018). Ambulatory Blood Pressure Reactivity as a Moderator in the Association Between Daily Life Psychosocial Stress and Carotid Artery Atherosclerosis. *Psychosomatic Medicine*, *Publish Ahead of Print*. https://doi.org/10.1097/PSY.0000000000000627

Kamarck, T. W., & Lovallo, W. R. (2003). Cardiovascular reactivity to psychological challenge: Conceptual and measurement considerations. *Psychosomatic Medicine*, *65*(1), 9–21.

Kasprowicz, A. L., Manuck, S. B., Malkoff, S. B., & Krantz, D. S. (1990). Individual Differences in Behaviorally Evoked Cardiovascular Response: Temporal Stability and Hemodynamic Patterning. *Psychophysiology*, *27*(6), 605–619. https://doi.org/10.1111/j.1469-8986.1990.tb03181.x

Kaur, M., Michael, J. A., Hoy, K. E., Fitzgibbon, B. M., Ross, M. S., Iseger, T. A., Arns, M., Hudaib, A.-R., & Fitzgerald, P. B. (2020). Investigating high- and low-frequency neuro-cardiac-guided TMS for probing the frontal vagal pathway. *Brain Stimulation*, *13*(3), 931–938. https://doi.org/10.1016/j.brs.2020.03.002

Khalsa, S. S., Adolphs, R., Cameron, O. G., Critchley, H. D., Davenport, P. W., Feinstein, J. S., Feusner, J. D., Garfinkel, S. N., Lane, R. D., Mehling, W. E., Meuret, A. E., Nemeroff, C. B., Oppenheimer, S., Petzschner, F. H., Pollatos, O., Rhudy, J. L., Schramm, L. P., Simmons, W. K., Stein, M. B., … Zucker, N. (2018). Interoception and Mental Health: A Roadmap. *Biological Psychiatry: Cognitive Neuroscience and Neuroimaging*, *3*(6), 501–513. https://doi.org/10.1016/j.bpsc.2017.12.004

Kragel, P. A., Han, X., Kraynak, T. E., Gianaros, P. J., & Wager, T. D. (2021). Functional MRI Can Be Highly Reliable, but It Depends on What You Measure: A Commentary on Elliott et al. (2020). *Psychological Science*, *32*(4), 622–626. https://doi.org/10.1177/0956797621989730

Kragel, P. A., Kano, M., Oudenhove, L. V., Ly, H. G., Dupont, P., Rubio, A., Delon-Martin, C., Bonaz, B. L., Manuck, S. B., Gianaros, P. J., Ceko, M., Losin, E. A. R., Woo, C.-W., Nichols, T. E., & Wager, T. D. (2018). Generalizable representations of pain, cognitive control, and negative emotion in medial frontal cortex. *Nature Neuroscience*, *21*(2), 283–289. https://doi.org/10.1038/s41593-017-0051-7

Krantz, D. S., & Manuck, S. B. (1984). Acute psychophysiologic reactivity and risk of cardiovascular disease: A review and methodologic critique. *Psychological Bulletin*, *96*(3), 435–464. https://doi.org/10.1037/0033-2909.96.3.435

Kraynak, T. E., MacCormack, J. K., Jennings, J. R., Critchley, H. D., Marsland, A. L., & Gianaros, P. J. (in prep). *Meta-analytic evidence for shared and specific functional neural correlates of cardiovascular stress reactivity and cardiac interoception (in prep)*.

Kraynak, T. E., Marsland, A. L., & Gianaros, P. J. (2018). Neural Mechanisms Linking Emotion with Cardiovascular Disease. *Current Cardiology Reports*, *20*(12), 128. https://doi.org/10.1007/s11886-018-1071-y

Kriegeskorte, N., Simmons, W. K., Bellgowan, P. S. F., & Baker, C. I. (2009). Circular analysis in systems neuroscience: The dangers of double dipping. *Nature Neuroscience*, *12*(5), 535–540. https://doi.org/10.1038/nn.2303

Krishnan, A., Woo, C.-W., Chang, L. J., Ruzic, L., Gu, X., López-Solà, M., Jackson, P. L., Pujol, J., Fan, J., & Wager, T. D. (2016). Somatic and vicarious pain are represented by dissociable multivariate brain patterns. *ELife*, *5*, e15166. https://doi.org/10.7554/eLife.15166

LeDoux, J. (2003). The emotional brain, fear, and the amygdala. *Cellular and Molecular Neurobiology*, *23*(4–5), 727–738.

Lindquist, K. A., Satpute, A. B., Wager, T. D., Weber, J., & Barrett, L. F. (2016). The Brain Basis of Positive and Negative Affect: Evidence from a Meta-Analysis of the Human Neuroimaging Literature. *Cerebral Cortex*, *26*(5), 1910–1922. https://doi.org/10.1093/cercor/bhv001

Makovac, E., Thayer, J. F., & Ottaviani, C. (2017). A meta-analysis of non-invasive brain stimulation and autonomic functioning: Implications for brain-heart pathways to cardiovascular disease. *Neuroscience & Biobehavioral Reviews*, *74*, 330–341. https://doi.org/10.1016/j.neubiorev.2016.05.001

Manuck, S. B., Kaplan, J. R., & Clarkson, T. B. (1983). Behaviorally Induced Heart Rate Reactivity and Atherosclerosis in Cynomolgus Monkeys: *Psychosomatic Medicine*, *45*(2), 95–108. https://doi.org/10.1097/00006842-198305000-00002

Marek, S., Tervo-Clemmens, B., Calabro, F. J., Montez, D. F., Kay, B. P., Hatoum, A. S., Donohue, M. R., Foran, W., Miller, R. L., Feczko, E., Miranda-Dominguez, O., Graham, A. M., Earl, E. A., Perrone, A. J., Cordova, M., Doyle, O., Moore, L. A., Conan, G., Uriarte, J., … Dosenbach, N. U. F. (2020). Towards Reproducible Brain-Wide Association Studies. *BioRxiv*, 2020.08.21.257758. https://doi.org/10.1101/2020.08.21.257758

Matthews, S. C., Paulus, M. P., Simmons, A. N., Nelesen, R. A., & Dimsdale, J. E. (2004). Functional subdivisions within anterior cingulate cortex and their relationship to autonomic nervous system function. *NeuroImage*, *22*(3), 1151–1156. https://doi.org/10.1016/j.neuroimage.2004.03.005

McEwen, B. S. (1998). Protective and Damaging Effects of Stress Mediators. *New England Journal of Medicine*, *338*(3), 171–179. https://doi.org/10.1056/NEJM199801153380307

Mills, P. J., & Dimsdale, J. E. (1991). Cardiovascular Reactivity to Psychosocial Stressors: A Review of the Effects of Beta-Blockade. *Psychosomatics*, *32*(2), 209–220. https://doi.org/10.1016/S0033-3182(91)72094-X

Morey, R. D., & Rouder, J. N. (2011). Bayes factor approaches for testing interval null hypotheses. *Psychological Methods*, *16*(4), 406–419. https://doi.org/10.1037/a0024377

Obrist, P. A. (1981). *Cardiovascular Psychophysiology: A Perspective*. Springer Science & Business Media.

Oppenheimer, S., & Cechetto, D. (2016). The insular cortex and the regulation of cardiac function. *Comprehensive Physiology*, *6*(2), 1081–1133. https://doi.org/10.1002/cphy.c140076

Oppenheimer, S. M., Wilson, J. X., Guiraudon, C., & Cechetto, D. F. (1991). Insular cortex stimulation produces lethal cardiac arrhythmias: A mechanism of sudden death? *Brain Research*, *550*(1), 115–121.

Parvizi, J., Rangarajan, V., Shirer, W. R., Desai, N., & Greicius, M. D. (2013). The Will to Persevere Induced by Electrical Stimulation of the Human Cingulate Gyrus. *Neuron*. https://doi.org/10.1016/j.neuron.2013.10.057

Petre, B., Woo, C.-W., Losin, E., Eisenbarth, H., & Wager, T. D. (2019). *Multilevel principal component regression for brain imaging*. Society for Neuroscience. https://www.abstractsonline.com/pp8/#!/7883/presentation/71055

Poldrack, R. A., Huckins, G., & Varoquaux, G. (2020). Establishment of Best Practices for Evidence for Prediction: A Review. *JAMA Psychiatry*, *77*(5), 534–540. https://doi.org/10.1001/jamapsychiatry.2019.3671

Pool, J. L., & Ransohoff, J. (1949). Autonomic effects on stimulating rostral portion of cingulate gyri in man. *Journal of Neurophysiology*, *12*(6), 385–392. https://doi.org/10.1152/jn.1949.12.6.385

Power, J. D., Barnes, K. A., Snyder, A. Z., Schlaggar, B. L., & Petersen, S. E. (2012). Spurious but systematic correlations in functional connectivity MRI networks arise from subject motion. *NeuroImage*, *59*(3), 2142–2154. https://doi.org/10.1016/j.neuroimage.2011.10.018

Power, J. D., Barnes, K. A., Snyder, A. Z., Schlaggar, B. L., & Petersen, S. E. (2013). Steps toward optimizing motion artifact removal in functional connectivity MRI; a reply to Carp. *NeuroImage*, *76*, 439–441. https://doi.org/10.1016/j.neuroimage.2012.03.017

Power, J. D., Schlaggar, B. L., & Petersen, S. E. (2015). Recent progress and outstanding issues in motion correction in resting state fMRI. *NeuroImage*, *0*, 536–551. https://doi.org/10.1016/j.neuroimage.2014.10.044

Pruessner, J. C., Dedovic, K., Khalili-Mahani, N., Engert, V., Pruessner, M., Buss, C., Renwick, R., Dagher, A., Meaney, M. J., & Lupien, S. (2008). Deactivation of the Limbic System During Acute Psychosocial Stress: Evidence from Positron Emission Tomography and Functional Magnetic Resonance Imaging Studies. *Biological Psychiatry*, *63*(2), 234–240. https://doi.org/10.1016/j.biopsych.2007.04.041

Rissman, J., Gazzaley, A., & D'Esposito, M. (2004). Measuring functional connectivity during distinct stages of a cognitive task. *NeuroImage*, *23*(2), 752–763. https://doi.org/10.1016/j.neuroimage.2004.06.035

Roy, M., Shohamy, D., & Wager, T. D. (2012). Ventromedial prefrontal-subcortical systems and the generation of affective meaning. *Trends in Cognitive Sciences*, *16*(3), 147–156. https://doi.org/10.1016/j.tics.2012.01.005

Ruiz Vargas, E., Sörös, P., Shoemaker, J. K., & Hachinski, V. (2016). Human cerebral circuitry related to cardiac control: A neuroimaging meta-analysis. *Annals of Neurology*, *79*(5), 709–716. https://doi.org/10.1002/ana.24642

Satterthwaite, T. D., Ciric, R., Roalf, D. R., Davatzikos, C., Bassett, D. S., & Wolf, D. H. (2019). Motion artifact in studies of functional connectivity: Characteristics and mitigation strategies. *Human Brain Mapping*, *40*(7), 2033–2051. https://doi.org/10.1002/hbm.23665

Satterthwaite, T. D., Elliott, M. A., Gerraty, R. T., Ruparel, K., Loughead, J., Calkins, M. E., Eickhoff, S. B., Hakonarson, H., Gur, R. C., Gur, R. E., & Wolf, D. H. (2013). An improved framework for confound regression and filtering for control of motion artifact in the preprocessing of resting-state functional connectivity data. *NeuroImage*, *64*, 240–256. https://doi.org/10.1016/j.neuroimage.2012.08.052

Satterthwaite, T. D., Wolf, D. H., Loughead, J., Ruparel, K., Elliott, M. A., Hakonarson, H., Gur, R. C., & Gur, R. E. (2012). Impact of in-scanner head motion on multiple measures of functional connectivity: Relevance for studies of neurodevelopment in youth. *NeuroImage*, *60*(1), 623–632. https://doi.org/10.1016/j.neuroimage.2011.12.063

Scheinost, D., Noble, S., Horien, C., Greene, A. S., Lake, E. MR., Salehi, M., Gao, S., Shen, X., O'Connor, D., Barron, D. S., Yip, S. W., Rosenberg, M. D., & Constable, R. T. (2019). Ten simple rules for predictive modeling of individual differences in neuroimaging. *NeuroImage*, *193*, 35–45. https://doi.org/10.1016/j.neuroimage.2019.02.057

Seeley, W. W. (2019). The Salience Network: A Neural System for Perceiving and Responding to Homeostatic Demands. *Journal of Neuroscience*, *39*(50), 9878–9882. https://doi.org/10.1523/JNEUROSCI.1138-17.2019

Shackman, A. J., Salomons, T. V., Slagter, H. A., Fox, A. S., Winter, J. J., & Davidson, R. J. (2011). The integration of negative affect, pain and cognitive control in the cingulate cortex. *Nature Reviews Neuroscience*, *12*(3), 154–167. https://doi.org/10.1038/nrn2994

Shenhav, A., Cohen, J. D., & Botvinick, M. M. (2016). Dorsal anterior cingulate cortex and the value of control. *Nature Neuroscience*, *19*(10), 1286–1291. https://doi.org/10.1038/nn.4384

Sheu, L. K., Jennings, J. R., & Gianaros, P. J. (2012). Test–retest reliability of an fMRI paradigm for studies of cardiovascular reactivity. *Psychophysiology*, *49*(7), 873–884. https://doi.org/10.1111/j.1469-8986.2012.01382.x

Sicorello, M., Herzog, J., Wager, T. D., Ende, G., Müller-Engelmann, M., Herpertz, S. C., Bohus, M., Schmahl, C., Paret, C., & Niedtfeld, I. (2021). Affective neural signatures do not distinguish women with emotion dysregulation from healthy controls: A mega-analysis across three task-based fMRI studies. *Neuroimage: Reports*, *1*(2), 100019. https://doi.org/10.1016/j.ynirp.2021.100019

Steptoe, A., & Vögele, C. (1991). Methodology of mental stress testing in cardiovascular research. *Circulation*, *83*(4 Suppl), II14-24.

Thayer, J. F., Åhs, F., Fredrikson, M., Sollers III, J. J., & Wager, T. D. (2012). A meta-analysis of heart rate variability and neuroimaging studies: Implications for heart rate variability as a marker of stress and health. *Neuroscience & Biobehavioral Reviews*, *36*(2), 747–756. https://doi.org/10.1016/j.neubiorev.2011.11.009

Thayer, J. F., & Lane, R. D. (2009). Claude Bernard and the heart–brain connection: Further elaboration of a model of neurovisceral integration. *Neuroscience & Biobehavioral Reviews*, *33*(2), 81–88. https://doi.org/10.1016/j.neubiorev.2008.08.004

Tibshirani, R. (1996). Regression Shrinkage and Selection via the Lasso. *Journal of the Royal Statistical Society. Series B (Methodological)*, *58*(1), 267–288.

Treiber, F. A., Kamarck, T., Schneiderman, N., Sheffield, D., Kapuku, G., & Taylor, T. (2003). Cardiovascular reactivity and development of preclinical and clinical disease states. *Psychosomatic Medicine*, *65*(1), 46–62.

Turner, A. I., Smyth, N., Hall, S. J., Torres, S. J., Hussein, M., Jayasinghe, S. U., Ball, K., & Clow, A. J. (2020). Psychological stress reactivity and future health and disease outcomes: A systematic review of prospective evidence. *Psychoneuroendocrinology*, *114*, 104599. https://doi.org/10.1016/j.psyneuen.2020.104599

Vogt, B. (2009). *Cingulate Neurobiology and Disease*. OUP Oxford.

Vul, E., Harris, C., Winkielman, P., & Pashler, H. (2009). Puzzlingly High Correlations in fMRI Studies of Emotion, Personality, and Social Cognition. *Perspectives on Psychological Science*, *4*(3), 274–290. https://doi.org/10.1111/j.1745-6924.2009.01125.x

Wager, T. D., Atlas, L. Y., Botvinick, M. M., Chang, L. J., Coghill, R. C., Davis, K. D., Iannetti, G. D., Poldrack, R. A., Shackman, A. J., & Yarkoni, T. (2016). Pain in the ACC? *Proceedings of the National Academy of Sciences*, *113*(18), E2474–E2475. https://doi.org/10.1073/pnas.1600282113

Wager, T. D., Atlas, L. Y., Leotti, L. A., & Rilling, J. K. (2011). Predicting Individual Differences in Placebo Analgesia: Contributions of Brain Activity during Anticipation and Pain Experience. *Journal of Neuroscience*, *31*(2), 439–452. https://doi.org/10.1523/JNEUROSCI.3420-10.2011

Wager, T. D., Atlas, L. Y., Lindquist, M. A., Roy, M., Woo, C.-W., & Kross, E. (2013). An fMRI-based neurologic signature of physical pain. *New England Journal of Medicine*, *368*(15), 1388–1397. https://doi.org/10.1056/NEJMoa1204471

Wager, T. D., van Ast, V. A., Hughes, B. L., Davidson, M. L., Lindquist, M. A., & Ochsner, K. N. (2009). Brain mediators of cardiovascular responses to social threat, Part II: Prefrontal-subcortical pathways and relationship with anxiety. *NeuroImage*, *47*(3), 836–851. https://doi.org/10.1016/j.neuroimage.2009.05.044

Wager, T. D., Waugh, C. E., Lindquist, M., Noll, D. C., Fredrickson, B. L., & Taylor, S. F. (2009). Brain mediators of cardiovascular responses to social threat: Part I: Reciprocal dorsal and ventral sub-regions of the medial prefrontal cortex and heart-rate reactivity. *NeuroImage*, *47*(3), 821–835. https://doi.org/10.1016/j.neuroimage.2009.05.043

Weiner, H. (1992). *Perturbing the Organism: The Biology of Stressful Experience*. University of Chicago Press.

Woo, C.-W., Chang, L. J., Lindquist, M. A., & Wager, T. D. (2017). Building better biomarkers: Brain models in translational neuroimaging. *Nature Neuroscience*, *20*(3), 365–377. https://doi.org/10.1038/nn.4478

Woo, C.-W., Koban, L., Kross, E., Lindquist, M. A., Banich, M. T., Ruzic, L., Andrews-Hanna, J. R., & Wager, T. D. (2014). Separate neural representations for physical pain and social rejection. *Nature Communications*, *5*. https://doi.org/10.1038/ncomms6380

Woo, C.-W., Roy, M., Buhle, J. T., & Wager, T. D. (2015). Distinct Brain Systems Mediate the Effects of Nociceptive Input and Self-Regulation on Pain. *PLOS Biology*, *13*(1), e1002036. https://doi.org/10.1371/journal.pbio.1002036

Wu, T., Snieder, H., & de Geus, E. (2010). Genetic influences on cardiovascular stress reactivity. *Neuroscience & Biobehavioral Reviews*, *35*(1), 58–68. https://doi.org/10.1016/j.neubiorev.2009.12.001

Yeo, B. T. T., Krienen, F. M., Sepulcre, J., Sabuncu, M. R., Lashkari, D., Hollinshead, M., Roffman, J. L., Smoller, J. W., Zöllei, L., Polimeni, J. R., Fischl, B., Liu, H., & Buckner, R. L. (2011). The organization of the human cerebral cortex estimated by intrinsic functional connectivity. *Journal of Neurophysiology*, *106*(3), 1125–1165. https://doi.org/10.1152/jn.00338.2011

Zhao, P., Rocha, G., & Yu, B. (2009). The composite absolute penalties family for grouped and hierarchical variable selection. *Annals of Statistics*, *37*(6A), 3468–3497. https://doi.org/10.1214/07-AOS584